2017

Reversal of the NPC Phenotype by START Domain Proteins

Tavis H. Sparrer
Virginia Commonwealth University

Reversal of the NPC Phenotype by START Domain Proteins

A Thesis submitted in partial fulfillment of requirements for a Master of Science degree at Virginia Commonwealth University.

By

Tavis H. Sparrer
B.S., Virginia Polytechnic Institute and State University, 2013

Director: Dr. Gregorio Gil,
Professor, Department of Biochemistry and Molecular Biology.

Virginia Commonwealth University
Richmond, Virginia
August, 2017

Acknowledgments

I would like to thank Dr. Gregorio Gil for his guidance and help over the course of my research, and my committee members Dr. Huiping Zhou and Dr. Phillip Hylemon. In addition, I would like to thank Dr. Daniel Rodriguez Agudo, Dr. William Pandak, and Dalila Marques, who have assisted and taught me throughout my research. I would also like to thank Julie Farnsworth for her assistance in our flow cytometry experiments.

Table of Contents

List of Tables

List of Figures

Abstract

REVERSAL OF THE NPC PHENOTYPE BY START DOMAIN PROTEINS

By Tavis H. Sparrer, M.S.

A Thesis submitted in partial fulfillment of requirements for the degree of a Master of Science degree at Virginia Commonwealth University.

Virginia Commonwealth University, 2017.

Major Director: Dr. Gregorio Gil, Professor, Department of Biochemistry and Molecular Biology

Niemann Pick Type C (NPC) disease is a fatal childhood neurological disease caused by mutations in the NPC-1 protein, resulting in cholesterol buildup in the late endosomes. StarD4 and StarD5 are cholesterol binding proteins that play a role in the intracellular cholesterol transport. In this study we overexpress StarD4 and StarD5 in *in vitro* and *in vivo* models, and find evidence of amelioration of the NPC phenotype. This study demonstrates that the overexpression of these proteins has the potential to be a therapeutic treatment for NPC disease.

Introduction & Background

Cholesterol and Atherosclerosis

Cholesterol is a sterol that plays an important role in mammal biology. It is an integral component of cellular membranes in mammals, and is responsible for maintaining membrane fluidity and integrity by intercalating itself between phospholipid molecules. Cholesterol is therefore needed for the synthesis of additional cellular membranes, and is necessary for cellular division. Cholesterol can be stored in lipid droplets as esterified cholesterol (EC) or can exist in cellular membranes as free cholesterol (FC). The plasma membrane of the cell has the highest concentration of free cholesterol, with 0.128 mg of cholesterol per mg of protein. Membranes of organelles have less- the Golgi body, endoplasmic reticulum, and mitochondria have 0.071, 0.014, and 0.003 mg/mg protein respectively [1]. Cholesterol is also converted into steroid hormones such as corticosteroids in the adrenal glands.

Cholesterol can be taken in through the diet or synthesized from acetyl-CoA in the endoplasmic reticulum (ER). This pathway includes the rate limiting step of cholesterol synthesis- the production of mevalonic acid from 3-hydroxy-3methylgutaryl-CoA (HMG-CoA) by HMG-CoA reductase [2]. Synthesis of cholesterol is particularly important in the brain, which is completely reliant on endogenous cholesterol produced in astrocytes. While diets in western countries tend to be high in cholesterol, the body has limited options of eliminating it.

Cholesterol is transported through the bloodstream via lipoproteins. These phospholipid monolayers enclose a hydrophobic compartment that is used to transport lipids through the blood. Embedded in this monolayer are apolipoproteins, which are used to interact with plasma membrane receptors. High Density Lipoprotein (HDL), which is synthesized in the liver, is

responsible for transport of cholesterol from the periphery and macrophages to the liver [3]. Transport into the liver is the primary mechanism of eliminating cholesterol from the body. In the liver, cholesterol is excreted into the bile or converted into bile acids [4]. Low Density Lipoprotein (LDL) is formed from Very Low Density Lipoprotein (VLDL), a lipoprotein synthesized by the liver mainly from endogenous lipids. LDL can be taken up by the liver, peripheral tissues or by macrophages by binding with the LDL receptor. LDL binding to LDL receptor allows it to be internalized by the cell by clatherin mediated endocytosis. LDL is then taken into lysosomes and cholesterol esters are hydrolyzed into free cholesterol.

SREBP-2 (Sterol Regulatory Element Binding Protein 2) is a transcription factor that upregulates genes involved in cholesterol synthesis and uptake [5]. SREBP-2 exists in an inactive form in the ER. In the absence of cholesterol or fatty acids, SREBP cleavage activating protein (SCAP) escorts SREBP-2 to the Golgi where it is cleaved, activated, and translocated to the nucleus. There, SREBP-2 activates the transcription of genes involved in cholesterol synthesis and uptake, such as HMG-CoA reductase and LDL receptor [6]. SREBP-1 is another sterol regulatory element binding protein, and has a mechanism of action is similar to SREBP-2. SREBP-1 is present in the ER and is cleaved in the absence of fatty acids and sterols [7]. Cleavage triggers transport to the Golgi and subsequent translocation to the nucleus where it activates the transcription of genes involved in fatty acid and lipid synthesis, such as Acetyl-CoA Carboxylase (ACC) and Fatty Acid Synthase (FAS) [8].

The health impacts of high circulating cholesterol can be severe and affect a large portion of the population. Macrophages take up cholesterol (associated with LDL) in the bloodstream and export this cholesterol to HDL [9]. If circulating macrophages become too laden with cholesterol, they transform into foam cells that collect along the walls of arteries in plaques and

can trigger a persistent inflammatory response. These 'coatheromatous plaques' contain necrotic tissue, extracellular lipids, and immune cells. This condition is known as atherosclerosis, and can lead to a variety of complications including stroke, myocardial infarction (heart attack) resulting from coronary artery disease, and peripheral artery disease. In addition, this enduring inflammatory response increases the risk of cancer, mainly by promoting angiogenic factors [10].

Despite age adjusted declines in atherosclerotic cardiovascular disease over the past two decades [11], heart disease is still the most common cause of death in the United States, killing about 610,000 people per year in the US [12]. The incidence rate remains high despite medical advances due to the high level of cholesterol in the western diet. Limiting cholesterol intake in the diet remains an effective form of prevention. Statins, such as mevinolin, are commonly prescribed to control plasma cholesterol levels, and have had limited success in reducing coatheromatous plaque volume [13]. Statins act as HMG-CoA reductase inhibitors, blocking cellular production of cholesterol. Low cholesterol levels in the ER cause the activation of SREBP2, which then upregulates LDL receptor. This leads to lower levels of LDL in the blood and reduces the risk of atherosclerosis. However, these drugs have can have a variety of side effects, including increased risks of muscular damage, hepatoxicity, stroke, and diabetes [14, 15]. Proprotein convertase subtilisin/kexin type 9 (PCSK9) inhibitors are another mechanism of treating atherosclerosis [16], and is now in use for extreme cases of the disease. PCSK9 degrades the LDL receptor, preventing peripheral cells from taking in and recycling LDL. PCSK9 inhibitors are monoclonal antibodies that bind to PCSK9, inhibiting it and preserving LDL receptor.

Theoretically, increasing levels of HDL should allow macrophages to export more cholesterol and prevent them from being embedded in artery walls. However, despite many

attempts at treating atherosclerosis by elevating HDL levels, so far this avenue of treatment has received mixed results [17]. This could be due to a lack of understanding of HDL subtypes and constituents, meaning more targeted treatments could see greater efficacy. Upregulating the cholesterol efflux pathway to HDL could also be an effective alternative treatment to atherosclerosis. Increasing the ability of macrophages to export cholesterol to HDL would prevent their deterioration into foam cells and reduce the formation of plaques. In addition, this could increase the elimination of cholesterol through bile acid synthesis by increasing HDL transport of cholesterol to the liver. However, the mechanism of cholesterol efflux is not completely understood.

ATP-Binding Cassette Transporter 1 (ABCA1) is the primary mechanism of cholesterol efflux. ABCA1 is a membrane bound protein that acts as a cholesterol pump, transporting intracellular cholesterol to lipoprotiens [18]. It has been shown that downregulation of ABCA1 in macrophages impairs cholesterol efflux and can lead to cardiovascular disease [19]. Tangier Disease, a genetic disorder characterized by very low levels of HDL, is caused by a mutation in ABCA1 [20]. ABCA1 transports cholesterol to lipoproteins by interacting with ApoA1, an apolipoprotein associated with both HDL and LDL. ABCA1 is upregulated by the Liver X Receptor (LXR), a nuclear transcription factor that acts as a receptor for oxysterols [5]. Oxysterols are produced in response to high free cholesterol levels, and in the presence of these cholesterol derivatives, LXR is activated [21]. It is not known how cholesterol is brought to ABCA1 to be transported out of the cell. Lipid rafts are regions of the plasma membrane that are high in cholesterol; these domains play important roles in signal transduction, and may be involved in cholesterol efflux. It has been shown that ABCA1 reduces free cholesterol content in

lipid raft domains [22]. However, the role of lipid rafts in ABCA1 mediated cholesterol efflux has been called into question [23].

Intracellular Cholesterol Transport

Cholesterol, when it is first taken in by the cell, is brought to the lysosomes and needs to be distributed throughout the cell. The intracellular transport of cholesterol is important for the uptake, efflux, and synthesis of cholesterol, and is necessary to maintain the fluidity and integrity of the various cellular membranes. While much of intracellular cholesterol transport is mediated by vesicles, non-vesicular mechanism represent a large portion of cholesterol transport and are poorly understood [24].

Among the best understood proteins that play a role in intracellular cholesterol transport is NPC-1. NPC-1 is a membrane bound protein found in the late endosomes. NPC-1 protein allows for the transport of cholesterol from the late endosomes to the ER by translocating cholesterol to outside the late endosome [25]. NPC-1 is upregulated by LXR [26]. Another well understood intracellular cholesterol transport protein is StarD1. StarD1 was the first member StarD protein family, which is characterized by the lipid binding StarD-related lipid transfer (START) domain. StarD1 is localized to and carries cholesterol to the mitochondria [27]. The homology of the START domain in StarD1 to the START domains of StarD4 and StarD5 led to the discovery of these two proteins and the StarD4 protein sub-family [28].

Both StarD4 and StarD5 have been shown to bind cholesterol *in vitro* [29]. The two proteins, being structurally dominated by their START domain, have a very high degree of structural homology. StarD4 has been shown to transport cholesterol to the ER [30, 31], though it is not clear if this transport is targeted to specific domain. It has also been linked to the production of cholesterol esters by Acyl-CoA: cholesterol acyltransferase (ACAT) and the formation of lipid droplets [31]. However, StarD4 has also been shown to play a role in the

transport of cholesterol between the plasma membrane and the endocytic recycling compartment (ERC), which regulates the recycling of endosomal contents to the plasma membrane [24]. It is clear that we do not yet have a complete picture of the role StarD4 plays in cholesterol transport.

StarD5 has a high level of expression in macrophages, which suggests that it may play a role in cholesterol efflux to HDL. It is also highly expressed in cancer cells, where high levels of cholesterol are needed for cell division. StarD5 is upregulated by the ER stress response via stabilization of StarD5 mRNA and by the ER stress transcription factor XBP-1 [32]. The ER is highly sensitive to changes in cholesterol metabolism, and changes in cholesterol homeostasis can cause ER stress. ER stress triggers the unfolded protein response (UPR), a process that is significant in many diseases [29, 32]. Both cholesterol and StarD5 move to the plasma membrane of the cell during ER stress or, as shown in unpublished data in our lab, exposed to lipoprotein deficient serum (LPDS). However there is no conclusive link between these two movements. The mechanism by which StarD5 moves to the plasma membrane is unknown, as are the proteins associated with StarD5, which could include chaperone proteins responsible for the movement of StarD5. It is possible that StarD5 transports cholesterol to ABCA1 for export, but this has not been confirmed.

Niemann Pick Type C Disease

The importance of the intracellular transport of cholesterol is most clear when errors in intracellular cholesterol transport cause disease. Niemann Pick Type C (NPC) disease is a fatal lysosomal cholesterol storage disease symptomatically identical but biochemically distinct from Niemann Pick Types A and B. While types A and B are the result of a deficiency in the Acid Sphingomyelinase protein, NPC is the result of a mutation in either the NPC-1 or NPC-2 protein that drastically reduces (but does not completely eliminate) its activity. NPC disease occurs in 1:150,000 people [33] and typically presents in early childhood, with half of cases occurring by 10 years of age. Symptomatically, NPC disease is primarily a neurodegenerative disease. It is characterized by dementia [34], ataxia [35], other progressive neurological problems, along with a swelling of the liver. The cerebellum, the portion of the brain responsible for motor control, is particularly affected by NPC [36].

Deficiency in NPC-1 results in cholesterol buildup in the lysosomes at the expense of other regions of the cell, including the ER. The low levels of cholesterol in the ER activate SREBP2, which upregulates the cholesterol biosynthesis pathway and causes overproduction of cholesterol. The cholesterol buildup from NPC in the late endosomes is recognizable in cells under a fluorescent microscope through filipin staining [37]. In addition, NPC should also decrease the levels of cholesterol in the plasma membrane and in the ER, and a decline in ER cholesterol should result in the increased expression of HMG-CoA reductase.

Treatment for NPC remains focused on managing symptoms and improving quality of life. Miglustat has been shown to have some effectiveness at slowing neurological deterioration [38], however no treatment has been developed that addresses the mechanism of NPC disease or

offers a chance of long term survival. There are a number of therapeutic strategies currently under research. Hydroxypropyl β-cyclodextrins (HP-β-CDs) have shown promise in reducing cholesterol in NPC-1 deficient cells [39]. This cyclic oligosaccharide contains a hydrophobic interior pocket that can extract cellular cholesterol. HP-β-CDs have had success in ameliorating the symptoms of NPC in animal and clinical trials, but have also been found to cause impaired hearing. N-butyldeoxynojirimycin [40], a glucoceramide synthase inhibitor, and histone deacetylase (HDAC) inhibitors have also been explored [41]. In particular, HDAC inhibitors have been successful in combination with 2-HP-β-CD and polyethylene glycol in mouse models [42]. HDAC inhibitors increase levels of NPC-1 protein, possibly through post-translational stabilization, which allows it to move outside of the ER.

Both StarD4 and NPC-1 are believed to facilitate cholesterol transport to the ER. This overlap in function raises the possibility that the overexpression of StarD4 could ameliorate the effects of NPC disease. Histochemistry of StarD4 knockout liver samples demonstrate that there are similarities between StarD4 knockouts and the NPC-1 mutant phenotype- both cells types visibly accumulate lipids (**Figure 1**). Our lab has also seen the similarities between phenotypes of NPC-1 mutant and StarD4 knockout cells under filipin staining, and have shown that overexpression of StarD4 with a StarD4 adenovirus reverses the phenotype in NPC-1 mutant cells (**Figure 2**). It is possible that this occurs because of StarD4 transport of lysosomal cholesterol to the ER, which would lower cholesterol synthesis to normal levels.

These results raise the possibility that overexpression of StarD4 could ameliorate the impacts of NPC disease. The overexpression of StarD5 could also potentially impact the NPC phenotype. Research into how these proteins function is crucial for understanding the intracellular transport of cholesterol as a whole, and is relevant to many diseases, including NPC

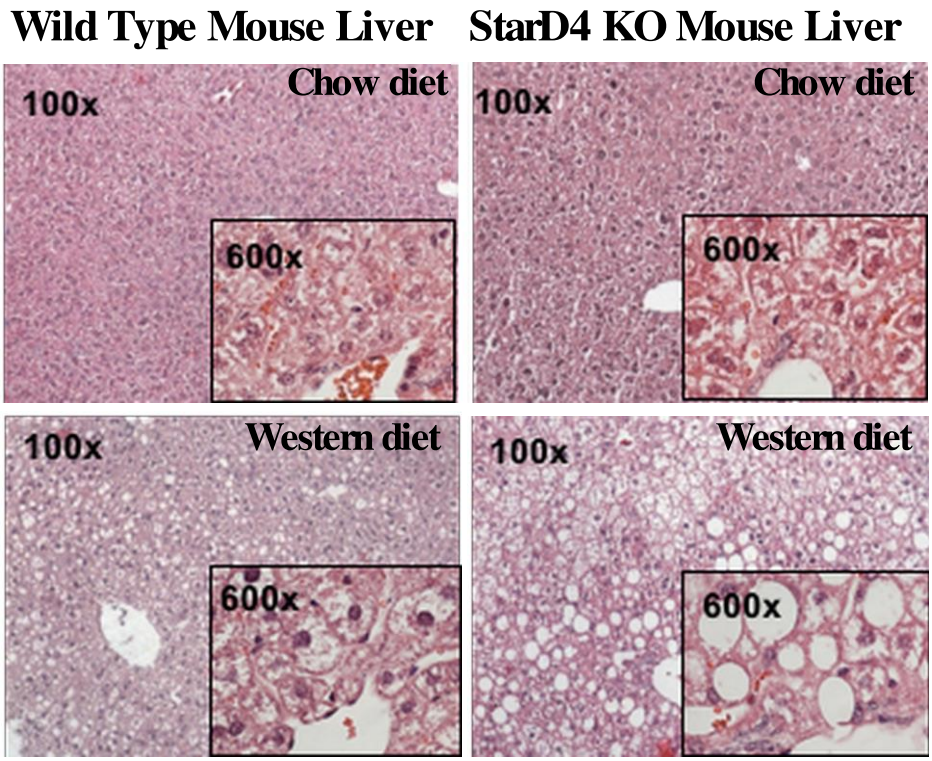

Figure 1. Histochemistry of WT and StarD4 KO mouse livers show lipid accumulation in StarD4 knockout livers. StarD4 knockout mice (right) have white spots indicating neutral lipids, which resembles what is seen in NPC-1 mutant cells. This accumulation of lipids is clearer under a high fat 'western diet', where mice have a greater accumulation of lipids than under a normal 'chow diet'.

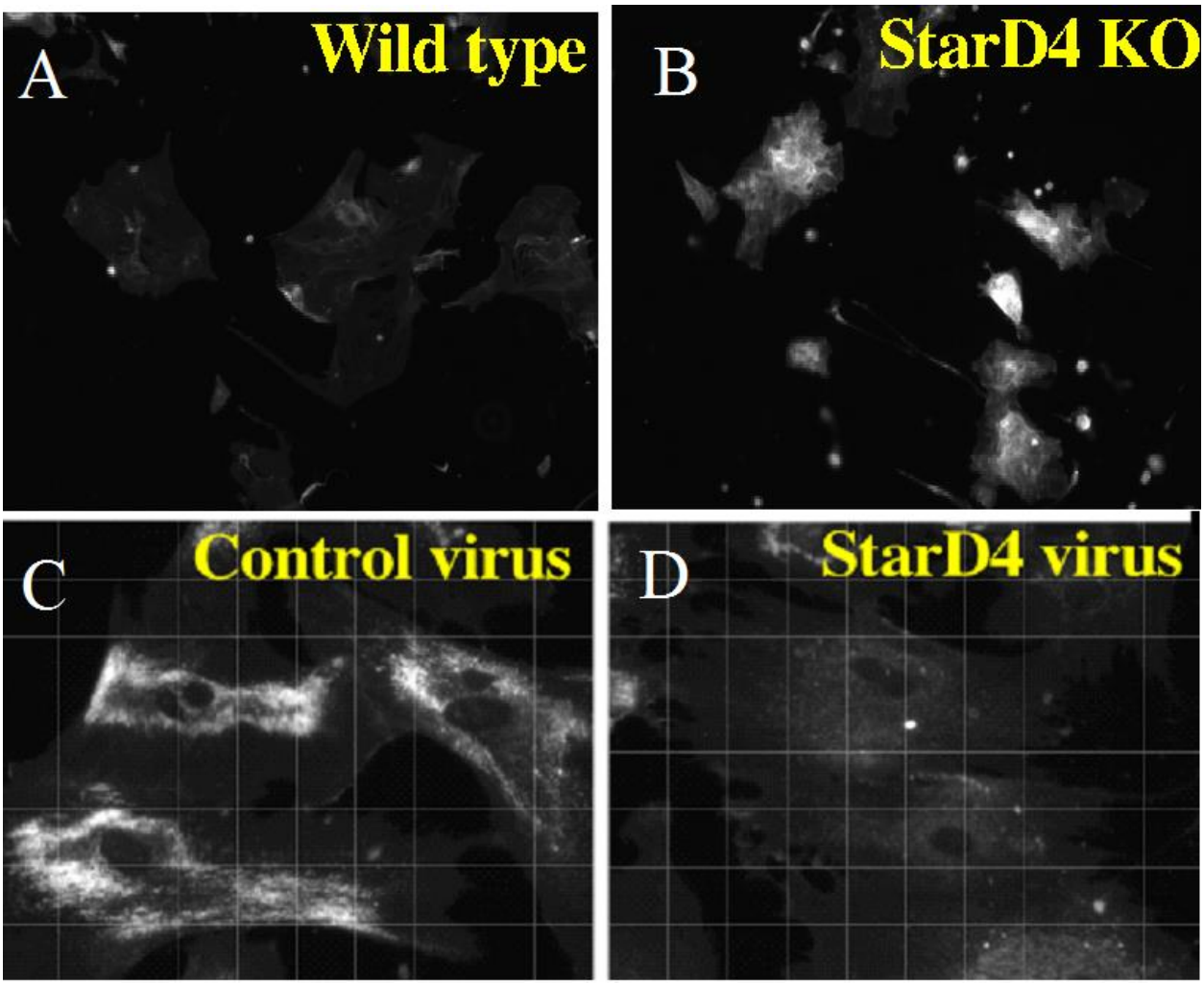

Figure 2. StarD4 overexpression normalizes cholesterol distribution in NPC-1 mutant fibroblasts. *Panel A* – Wild type astrocytes have low levels of free cholesterol under filipin staining. *Panel B* – StarD4 knockout astrocytes higher levels of intracellular free cholesterol, similar to NPC-1 mutant cells. *Panel C* – NPC-1 mutant fibroblasts infected with a control adenovirus also have high levels of free cholesterol, similar to in StarD4 knockout astrocytes. *Panel D* – Free cholesterol levels in NPC-1 mutant fibroblasts is lower after infection with a StarD4 adenovirus.

Materials & Methods

Materials

C57 BL/6J NPC-1 Mutant (nmf164) mice were ordered from Jackson Labs. Cell lines used include HeLa cells and Chinese Hamster Ovary (CHO) wild type and 10-3 NPC-1 mutant cells from the Liscum lab [43]. Primers and fluorescent probes for qPCR were ordered from Integrated DNA Technologies **(Table 1).** Other general chemicals used were ordered from Sigma.

Table 1. Primers and probes used for qRT-PCR experiments.

Gene Name	ID	Primer	Nucleotides	Sequence
Mouse NPC-1	NM_008720	Fwd. Primer	1684-1707	CAAGTAGGCGACGACTTCTATATC
Mouse NPC-1	NM_008720	Rev. Primer	1764-1783	CGT GGAGCAAACTCGTATCA
Mouse NPC-1	NM_008720	Probe	1723-1748	ACACACTTTCTGTACTGTGTACGGGC
Mouse StarD5	NM_023377.4	Fwd. Primer	250-271	CGGGAGAAGTGGGATGATAATG
Mouse StarD5	NM_023377.4	Rev. Primer	354-375	CACAAAGTCCCTGGGAGAAATA
Mouse StarD5	NM_023377.4	Probe	301-324	ACGGATATGCTGTGTGTGAGCAGA
Human StarD4	NM_001308056.1	Fwd. Primer	370-391	CTCTACAAAGCCCAAGGTGTTA
Human StarD4	NM_001308056.1	Rev. Primer	448-468	AGTCATCAAGCTGTCCCAATC
Human StarD4	NM_001308056.1	Probe	415-438	ATAGACCATATACGCCCAGGGCCT
Mouse ABCA1	NM_013454	Fwd. Primer	5899-5920	GGGTGGTGTTCTTCCTCATTAC
Mouse ABCA1	NM_013454	Rev. Primer	5984-6005	CACATCCTCATCCTCGTCATTC
Mouse	NM_013454	Probe	5952-5975	CCCAGACCTGTAAAGGCGA

ABCA1				AGCTT
Mouse HMGCR	BC085083	Fwd. Primer	1893-1915	CTGAAGGGTTTGCAGTGATAAAG
Mouse HMGCR	BC085083	Rev. Primer	1987-2008	CCTGGACTGGAAACGGATATAG
Mouse HMGCR	BC085083	Probe	1917-1940	AGGCCTTTGATAGCACCAGCAGAT
Mouse SREBP1	NM_001313979.1	Fwd. Primer	2041-2060	GCGGCTGTTGTCTACCATAA
Mouse SREBP1	NM_001313979.1	Rev. Primer	2102-2122	CCAGGTTAGAAGCAGCAAGAT
Mouse SREBP1	NM_001313979.1	Probe	2075-2097	ATGCCATGGGCAAGTACACAGGA
Mouse SREBP2	AF374267.2	Fwd. Primer	1327-1345	TGGATGACGCAAAGGTCAA
Mouse SREBP2	AF374267.2	Rev. Primer	1403-1424	CAGGAAGGTGAGGACACATAAG
Mouse SREBP2	AF374267.2	Probe	1346-1369	ACAGGAGGAGAGTCCGGTTCATCC
Mouse FAS	NM_007988	Fwd. Primer	3523-3544	GCTATGATTATGGCCCTCAGTT
Mouse FAS	NM_007988	Rev. Primer	3600-3621	CCATGAAGGTCACCCAGTTATC
Mouse FAS	NM_007988	Probe	3568-3591	TTGAAGGTGAACAAGGCAAGCTGC
Mouse ACC	NM_133360.2	Fwd. Primer	6166-6187	GTTTCTCTGGTGGGATGAAAGA
Mouse ACC	NM_133360.2	Rev. Primer	6256-6275	GGGCGGGATGTAAACCATTA
Mouse ACC	NM_133360.2	Probe	6221-6244	CATTGTGGATGGCTTGCGGGAATG
Mouse GAPDH	NM_001289726	Fwd. Primer	833-853	GGAGAAACCTGCCAAGTATGA
Mouse GAPDH	NM_001289726	Rev. Primer	904-922	TCCTCAGTGTAGCCCAAGA
Mouse GAPDH	NM_001289726	Probe	859-882	TCAAGAAGGTGGTGAAGCAGGCAT

Virus Preparation

To create the StarD4-AAV9 virus (**Figure 3)**, the coding region of human StarD4 cDNA was excised from the RC223123 plasmid (Origen) by EcoR1/XhoI digestion. This fragment was inserted after a CMV promotor into the pAAV-IRES-hrGFP plasmid **(Figure 4)**, which contains the inverted repeats needed to make the AAV9 virus. This insertion was confirmed by HindIII, EcorR1/XhoI, NotI, and SmaI digestion **(Figure 5)**. Both a control and StarD4-AAV9 virus were ordered from the Penn Vector Core. The AAV9 serotype was chosen for its ability to infect both the liver and the brain, its ability to remain active for over a month post injection, and its low inflammatory effect [44].

StarD1, StarD4, StarD5, and control adenoviruses were commonly used in the lab. In the StarD1, StarD4, and StarD5 adenoviruses, the transcription of cDNA encoding the StarD protein was driven by the human CMV promoter [45].

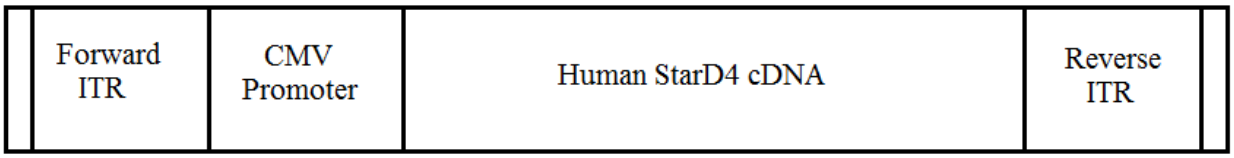

Figure 3. A scheme of the plasmid used to make the AAV9-StarD4 virus.

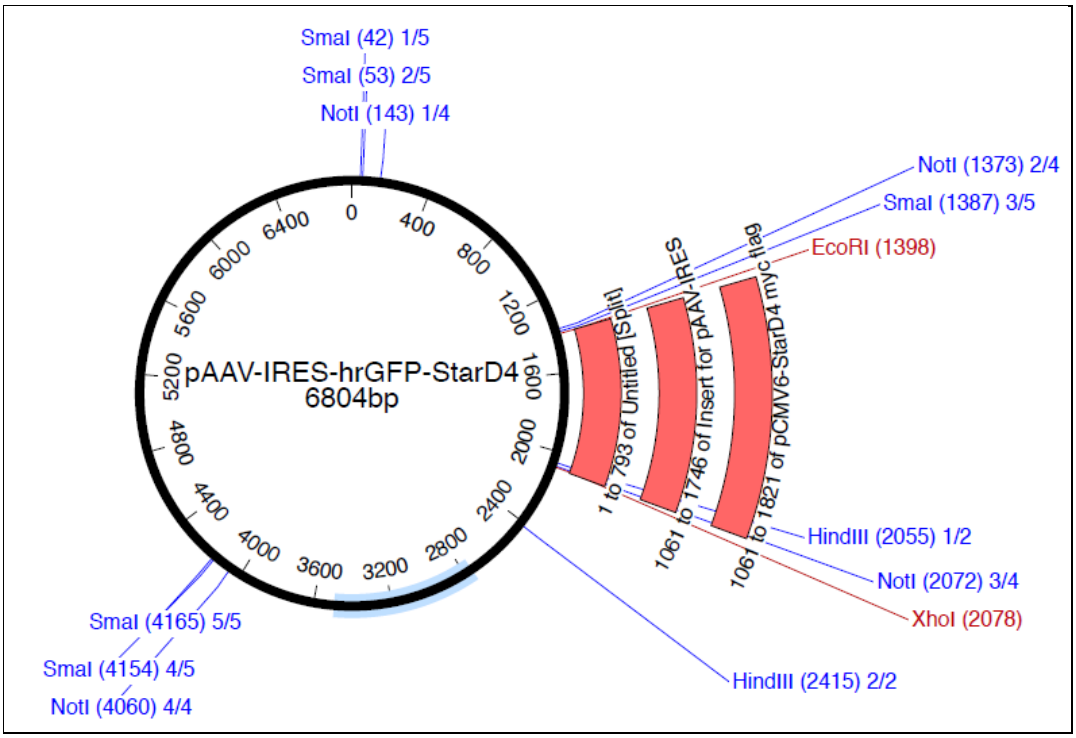

Figure 4. Insertion of the StarD4 cDNA fragment into the pAAV-IRES-hrGFP plasmid.

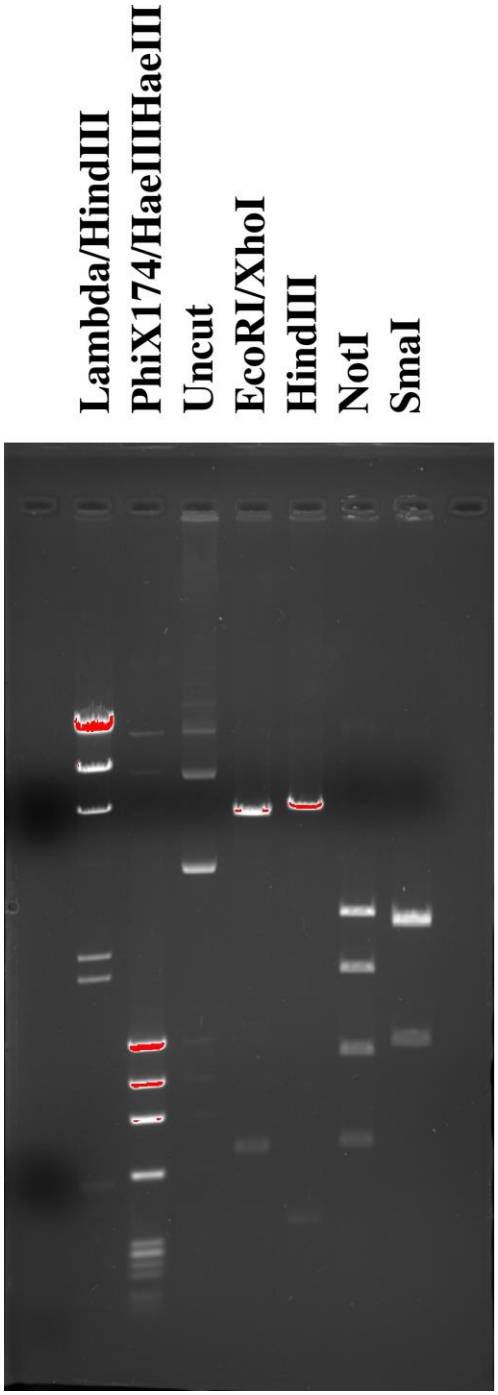

Figure 5. Restriction enzyme analysis of the pAAV-IRES-hrGFP-StarD4 plasmid by digestion with EcoR1/XhoI, HindIII, NotI, and SmaI.

StarD5$^{-/-}$ Mice Experiments

Wild type and StarD5$^{-/-}$ C57 BL/6J mice were fed a normal chow diet, a 2% cholesterol diet for 5 days, or a Western Diet (the TD.88137 adjusted calories diet) for 8 weeks. Livers were harvested and RNA was extracted. qRT-PCR was used to determine relative mRNA expression. Peritoneal macrophages from wild type and StarD5$^{-/-}$ C57 BL/6J mice were harvested and RNA was extracted for qRT-PCR.

Overexpression of StarD4 in NPC-1 Mutant Mice

NPC-1 nmf164 mutant mice were infected with $4x10^{12}$ pfu of StarD4-AAV9 virus or a control virus using the orbital injection technique. Four weeks following the first injection, the mice were injected with another $4x10^{12}$ pfu of StarD4 AAV9 virus. Ten days after each injection, mice were tested for motor ability with the coat hanger test. Uninjected NPC-1 mutant and wild type mice were also tested. Mice were allowed to grip a coat hanger suspended 8 inches above a counter top, and were allowed to hang until they fell off. If a mouse was able to hang on for at least 2 minutes they were let down and 2 minutes was marked as their hang time (**Figure 6**). Six weeks following the first injection, the mice were killed via cervical dislocation and weighed. The brains and livers were harvested, and samples were used for cholesterol and triglyceride quantifications and mRNA profiling by qRT-PCR.

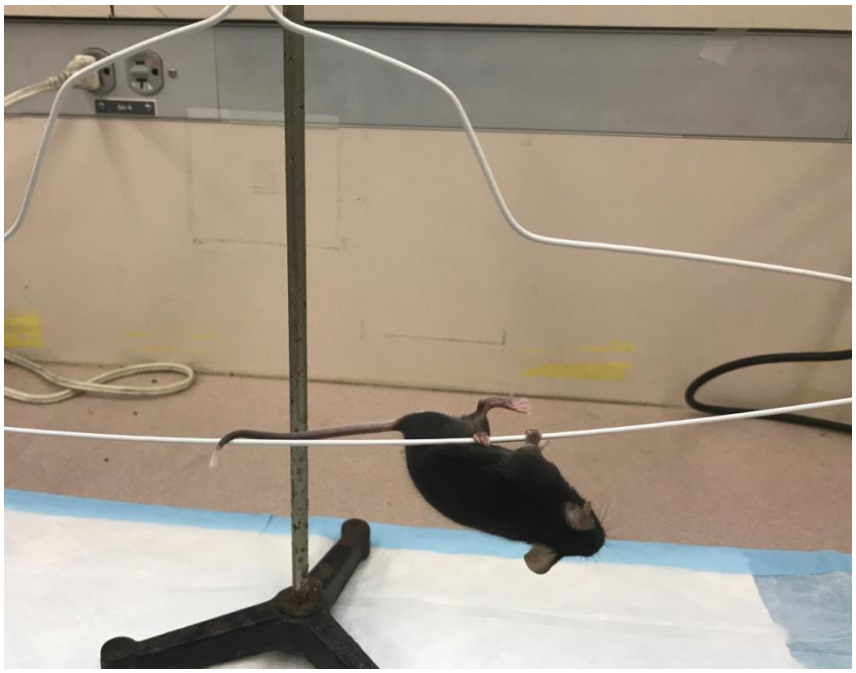

Figure 6. The coat hanger test.

RNA Extraction

RNA was harvested with either an RNeasy Plus Mini Kit (Quiagen) according to the protocol provided by the kit, or with Trizol reagent (Ambion). For samples harvested with Trizol reagent, 25 ng of tissue was weighed, homogenized, and incubated in 500 µL of Trizol reagent for 5 minutes. 100 µL of chloroform was added to lysate, and incubated for 3 minutes. Samples were spun down for 15 minutes at 12,000 rcf at 4 °C. The upper aqueous phase was transferred to a new tube and 250 µL of isopropanol was added. These samples were incubated for 10 minutes and then spun down for 10 minutes at 12,000 rcf at 4 °C. The pellet was washed in 75% ethanol and spun down again for 5 minutes at 7,500 rcf at 4 °C. The supernatant was removed and the pellet was left to dry for 10 minutes, before being resuspended in 50 µL of RNase free water. The RNA from both extraction methods was quantified on a Nanodrop 2000c (Thermo).

mRNA Quantification

qRT-PCR was run with the Brilliant III Ultra-Fast QRT-PCR Master Mix kit (Agilent). Each set of primers was calibrated using temperature and concentration curves. 500 nM of EDTA was added to mixes for each gene except human StarD4. GAPDH was used as an internal control for all samples, except human StarD4, where it was used as an external control. qRT-PCR was run on a Realtime qPCR Cycler (CFX96, BioRad).

Total Cholesterol, Free Cholesterol, Triglyceride Quantification

Samples of livers and brains were suspended in lysis buffer at a ratio of 100 mg of tissue per 700 µL of buffer, homogenized and lysed. 150 µL of the homogenates were then suspended in 5 mL of 2:1 chloroform: methanol and incubated overnight. The samples were spun down and the supernatant was aliquoted for use in lipid assays. 100 µL of each sample was dried under N_2 and used in kit assays for cholesterol (Cholesterol E, Wako), free cholesterol (Free Cholesterol E, Wako), and triglycerides (Infinity Triglycerides, Thermo) following kit protocols. A Bradford assay with BSA standards was used to quantify protein concentrations of the lysates. This data was used to determine cholesterol and triglyceride concentrations per µg of protein.

Protein Quantification

Bradford Assays were used to determine protein concentrations. We used BioRad Protein Assay Dye Reagent Concentrate diluted 1:5 in water as a Bradford reagent. Bovine Serum Albumin (BSA) was used as a protein standard. The absorbance of the samples was measured using a Biomate 3 Spectrophotometer at 595 nm (Thermo).

Production of fALOD4 Cholesterol Probe*

A fluorescent probe was used to quantify accessible plasma membrane free cholesterol [46, 47]. We used ALOD4, the cholesterol binding fourth domain of the ALO protein from *Bacillus anthracis*. In this experiment we used an ALOD4 mutant (ALOD4*) with two point mutations (S404C and C472A), along with a His_6 tag at the NH_2-end. These mutations allow ALOD4* to more effectively bind to a fluorophore. Competent *E. Coli* cells were transformed using a plasmid containing the ALOD4* sequence in front of the T7 promotor, which was given to us by Dr. Arun Radhakrishnan [48]. Viable colonies were grown out to 6 L and induced with 1 mM IPTG at 30 °C for 16 hours. T7 polymerase is present in the genome of this *E. Coli* strain and is regulated by the Lac operon. IPTG, a lactose mimic, induces production of T7 by binding to the repressor, LacI. T7 will then rapidly transcribe ALOD4*, giving high yields of the protein.

The cells were spun down at 5,000 rpm for 20 minutes and harvested in 120 mL of Buffer B (50 mM Tris, 150 mM NaCl, 1mM DTT, 1mg/mL Lysozyme, 1X Pefabloc SC, and 0.5X Protease Inhibitor Cocktail). Cells were lysed with a dounce homogenizer and then by a tip sonicator (550 Sonic Dismembrator, Fisher Scientific) using five 30-second pulses up to setting #7. The lysate was spun down for 1 hour at 45,000 rpm and the protein containing supernatant was collected. 2 mL of an Ni-NTA agarose gel was washed in Buffer B with 50 mM imidazole and the cell lysate was run through the Ni-NTA gel twice to capture ALOD4* protein. The agarose gel was then washed with 20 mL of Buffer B with 50 mM imidazole and the protein was eluted with 20 mL of Buffer B with 400 mM imidazole. 2 mL elution fractions were collected and along with original lysate and flowthrough, were run on a 12% Acrylamide gel and stained with coomassie blue dye. The elutions containing ALOD4* were pooled and the imidazole

concentration was diluted to 50 nM via filtration using the Amicon Ultra-15 Centrifuge Filter kit (Millipore). The pooled sample was run through a Ni-NTA column again, and eluted in 400 nM imidazole. Protein was labelled with fluorescent Alexa Fluor 488 C_5-maleimide dye by rotating 200 nmol of protein with 1400 nmol of fluorescent dye overnight at 4°C. Fluorescently labelled ALOD4* is referred to as fALOD4*. Unbound dye was removed by concentration and dilution using the Amicon Ultra-15 Centrifuge Filter kit (Millipore). In order to ensure that the fluorescent dye bound to ALOD4*, fALOD4* was run on two 12% acrylamide gels. One gel was stained with coomassie blue; the other was fluorescently imaged with a ChemiDoc MP Imaging System (BioRad).

*Quantification of Plasma Membrane Cholesterol by FACS Analysis of fALOD4**

Wild type CHO and NPC-1 10-3 mutant cells were harvested in 0.25% trypsin or Accutase cocktail (eBioscience) and suspended in Buffer D (PBS with 1mM EDTA and 2% LPDS) at a concentration of 1 million cells per mL. Cells were incubated by rotating with the indicated amounts of fALOD4* for 3 hours at 4 °C in darkness. The fluorescently labelled cells were washed with PBS, spun down for 2.5 minutes at 2,5000 rcf, and suspended in PBS for flow cytometry (FACS) analysis.

Overexpression of StarD5 in NPC-1 Mutant Mice

NPC-1 mice were injected with a total of $4.23x10^{10}$ of StarD5 adenovirus by five orbital injections over the course of three days. Three and seven days after the first injection, the livers of these mice were harvested for cholesterol/triglyceride quantification and qRT-PCR.

Protein Detection by Western Blot

Protein samples were denatured in sample buffer (20 mM Tris, 114 mM β-Mercaptoethanol, 6% Glycerol, 0.002% Bromophenol Blue, and 2.1% SDS), boiled for 10 minutes, and loaded into a 12% acrylamide gel. The protein was run on the gel in running buffer (25 mM Tris, 190 mM glycine, 0.1% SDS) for 25 minutes at 120V and 25 minutes at 160V. An immunobilon-P membrane was soaked in methanol for 5 minutes and transfer buffer (25 mM Tris, 190 mM glycine, 20% methanol) for 5 minutes. The proteins were then transferred to the membrane in transfer buffer for 50 minutes at 11V using a semi-dry transfer method.

Membranes were blocked in PBS with 0.1% Tween 20 (PBST) and 5% Instant Nonfat Dry Milk (Nestle) for 2 hours and incubated with a primary antibody in PBST with 2.5% Instant Nonfat Dry Milk at 4 °C overnight. Membranes were washed three times in PBST for 10 minutes each and incubated in PBST with Instant Nonfat Dry Milk and a secondary antibody for 1 hour at room temperature. Membranes were washed three times in PBST for 10 minutes each and incubated for 1 minute in darkness in Western Lighting reagents (Perkins-Elmer). Images were taken with the chemi-high resolution mode on the Chemi-Dock XLS+ (BioRad).

Protein Detection by Coomassie Stain

Protein samples were denatured in Sample buffer, boiled for 10 minutes, and loaded into a 12% acrylamide gel. These samples were run on the gel in running buffer for 30 minutes at 120V. The gel was incubated in fixing solution (50% methanol, 10% acetic acid) for 1 hour, and stained in staining solution (0.1% Coomassie Blue R-250, 50% methanol, 10% acetic acid) for 20 minutes. The gel was then destained in destaining solution (40% methanol, 10% acetic acid),

decanting as solution becomes colored, and left to destain overnight. Imaging was done on the Chemi-Dock XLS+ (BioRad) with the coomassie stain mode.

Immunoprecipitation (IP)

HeLa cell cultures were infected with 2000 viral particles of StarD5 adenovirus and incubated in either 10% FBS or 10% LPDS media. HeLa cells were also infected with 2000 viral particles of a control adenovirus and incubated in 10% FBS media. Cells were harvested by scraping in PBS, and some samples were crosslinked with formaldehyde to link StarD5 to any associated proteins. To crosslink, cells were suspended PBS with 1% formaldehyde for 10 minutes at a concentration of $1x10^7$ cells per mL. Formaldehyde was quenched with PBS with 125 mM glycine. All samples were then lysed with Lysis Buffer (20mM Tis-HCl, 150mM NaCl, 1mM EDTA, 0.5% NP40 pH 7.4, and 1% protease inhibitor cocktail from Bimake).

To isolate StarD5 and its potential chaperones, the lysate was then purified via an immunoprecipitation process. The lysate was cleaned by rotating 600 µL of lysate with 40 µL of an anti-HA agarose gel (Sigma) for 30 minutes at 4 °C. Then the lysate was passed through 40 µL of anti-flag affinity gel (Bimake) overnight at 4 °C to capture StarD5 and associated proteins. The agarose was washed three times with 500 µL of Lysis Buffer and eluted with 150 ng/µL Flag Peptide (Sigma-Aldrich) by rotating for 30 minutes at 4 °C. The agarose was then treated with sample buffer and boiled for 10 minutes to collect any remaining protein. Samples were then run on a 12% acrylamide gel and stained with coomassie dye.

Results

My research consists of four projects. 1- The characterization of mRNA expression profiles in StarD5$^{-/-}$ mice. 2- Exploration of the potential use of StarD4 to ameliorate the NPC phenotype *in vivo*, and investigating StarD4 overexpression as a potential therapy. 3- Exploration of the potential of StarD5 to overcome the NPC phenotype in both *in vitro* and *in vivo* models. 4- Beginning the process of characterizing potential chaperone proteins for StarD5.

1- Wild Type and StarD5$^{-/-}$ Mice Have Different Gene Expression Profiles

Genes Involved in Cholesterol Metabolism and Transport Have Altered mRNA Expression in StarD5$^{-/-}$ Mouse Livers

As a part of the characterization of StarD5$^{-/-}$ mice developed in our lab, we extracted RNA from the livers of wild type and StarD5$^{-/-}$ mice. The relative mRNA expression of key genes involved in cholesterol metabolism and transport were quantified by qRT-PCR **(Figure 7)**. As expected, StarD5$^{-/-}$ mouse livers had no expression of StarD5 mRNA. mRNA expression in StarD5$^{-/-}$ mouse livers was significantly different from in wild type livers for four other genes, ABCA-1, HMG-CoA reductase, NPC-1, and FAS. StarD5$^{-/-}$ mouse livers have a higher level of expression of ABCA-1 than in wild types– 160% of wild type livers. StarD5$^{-/-}$ mouse livers also have a higher level of NPC-1 expression, at 210% of wild type liver expression. Other genes had lower levels of expression in StarD5$^{-/-}$ mouse livers, like HMG-CoA reductase where StarD5$^{-/-}$ mice had 70% of the expression of wild type livers. FAS mRNA expression in StarD5$^{-/-}$ mouse livers was 50% of wild type expression. In the other genes we tested, wild type and StarD5$^{-/-}$

mouse livers did not have significant differences in mRNA expression. These genes include SREBP2, where StarD5$^{-/-}$ mouse livers had about 125% of the mRNA expression of wild types. StarD5$^{-/-}$ mouse livers had 160% of the mRNA expression of ACC and 230% of the expression of StarD4 compared to wild type livers, however these differences were not statistically significant.

Genes Involved in Cholesterol Metabolism and Transport do not Have Altered mRNA Expression in StarD5$^{-/-}$ Mouse Macrophages

RNA was also extracted from macrophages harvested from wild type and StarD5$^{-/-}$ mice. qRT-PCR was used to quantify the relative mRNA expression of genes involved in cholesterol transport and metabolism. We found wild type and StarD5$^{-/-}$ macrophages did not have significantly different mRNA expressions in any of the genes we tested **(Figure 8)**. In StarD5$^{-/-}$ macrophages, ABCA-1 HMG-CoA reductase, SREBP1, SREBP2, NPC-1, and ACC had 140%, 130%, 90%, 100%, 90%, and 140% of the mRNA expression found in wild types.

StarD5$^{-/-}$ and Wild Type Mice Have Similar mRNA Expression Profiles Under a High Cholesterol Diet

We next tested how gene expression changed in response to diet in wild type and StarD5$^{-/-}$ mice. StarD5$^{-/-}$ and wild type mice were fed either a western diet for 8 weeks or a 2% cholesterol diet for 5 days. RNA was extracted from the livers of these mice, and the mRNA concentration of genes involved in cholesterol transport and metabolism was quantified using qRT-PCR. In mice that were fed a 2% cholesterol diet, we found that while the mRNA expression profile changed compared to mice that had been fed a chow diet **(Figure 9)**, wild type and StarD5$^{-/-}$ mice had very similar levels mRNA expression for all genes tested **(Figure 10)**.

This pattern holds true even for genes where StarD5$^{-/-}$ and wild type mice had very different levels of mRNA expression in wild type mice. In addition, we see that several genes, such as FAS, are less sensitive to changes in the cholesterol content of the diet. In wild type mice FAS mRNA expression drops 5-fold in mice fed a 2% cholesterol diet, while in NPC-1 mutant mice FAS mRNA expression increases by 20% in mice fed a 2% cholesterol diet.

In the livers of mice that were fed a western diet, we again saw the expected changes in mRNA expression compared to mice that were fed a chow diet. We also found that in three genes, wild type StarD5$^{-/-}$ mice differed in mRNA expression. For SREBP2, we found that the livers StarD5$^{-/-}$ mice had 50% the mRNA expression of wild type mice. For ACC, we found that the livers of StarD5$^{-/-}$ mice had 260% the mRNA expression of wild type mice. For FAS, the livers of StarD5$^{-/-}$ mice had 70% the mRNA expression of FAS that we found in wild type mice.

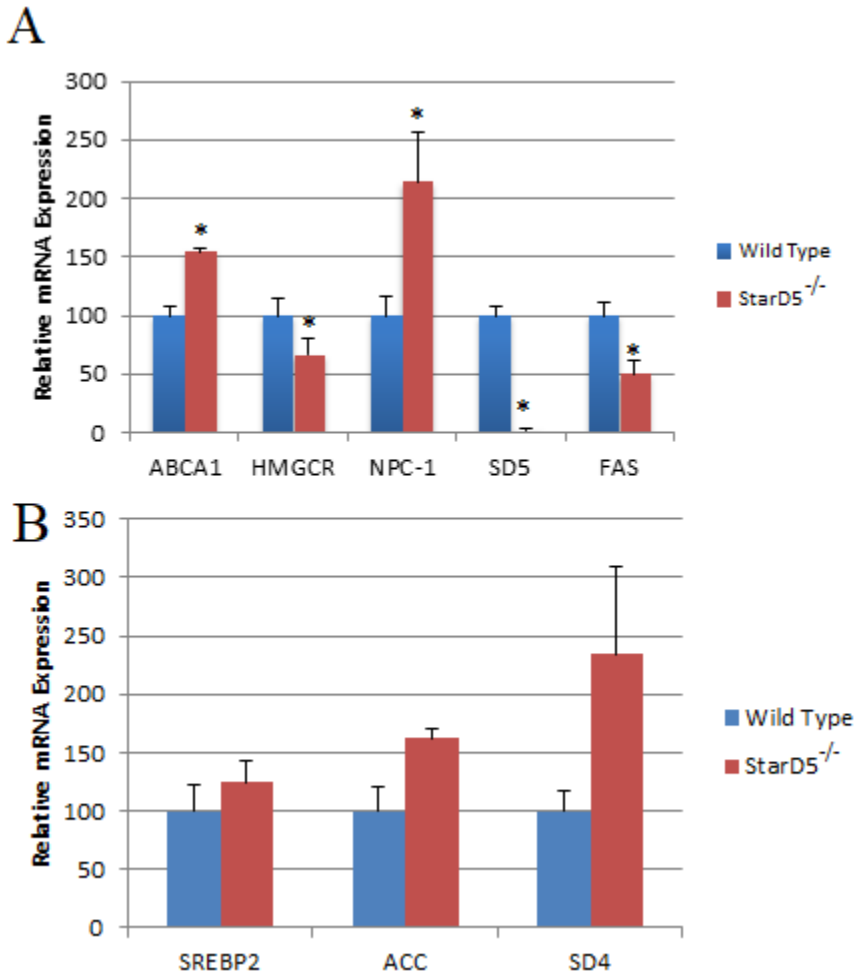

Figure 7. Relative mRNA expression levels in StarD5$^{-/-}$ and wild type livers. *Panel A*- ABCA1, HMG-CoA reductase, NPC-1, StarD5, and FAS mRNA expression levels. *Panel B*- SREBP2, ACC, and StarD4 mRNA expression levels. * - P<0.1. n = 3.

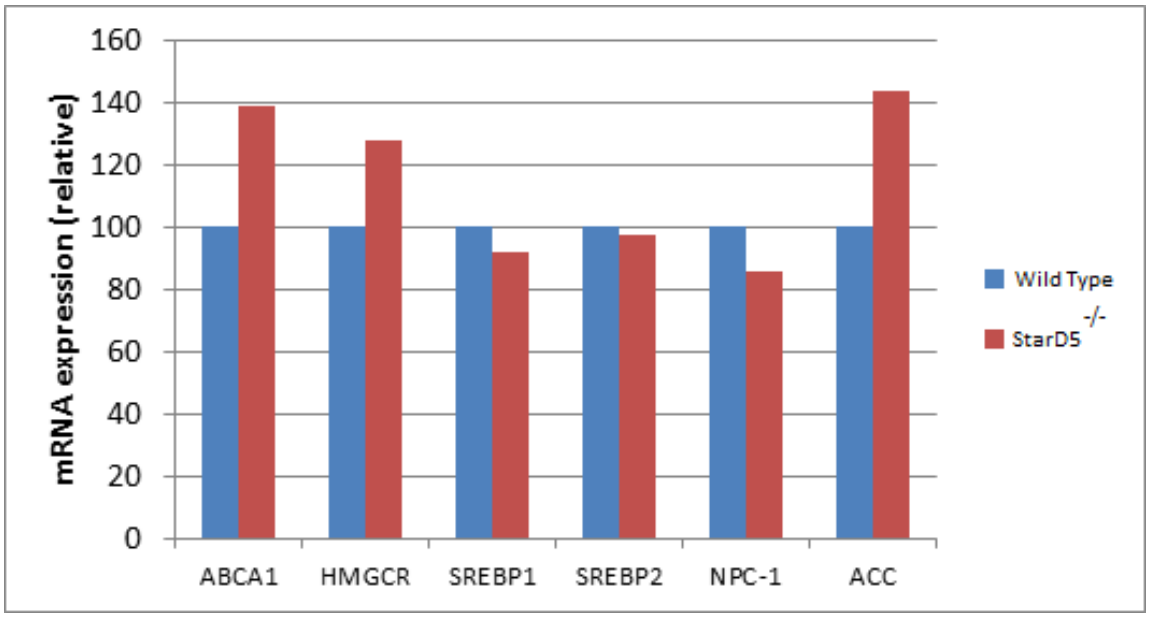

Figure 8. Relative mRNA expression in StarD5$^{-/-}$ and wild type macrophages. Relative mRNA expressions of ABCA1, HMG-CoA reductase, SREBP1, SREBP2, NPC-1, and ACC. None of the genes tested showed a statistically significant change in mRNA expression in macrophages. n = 1.

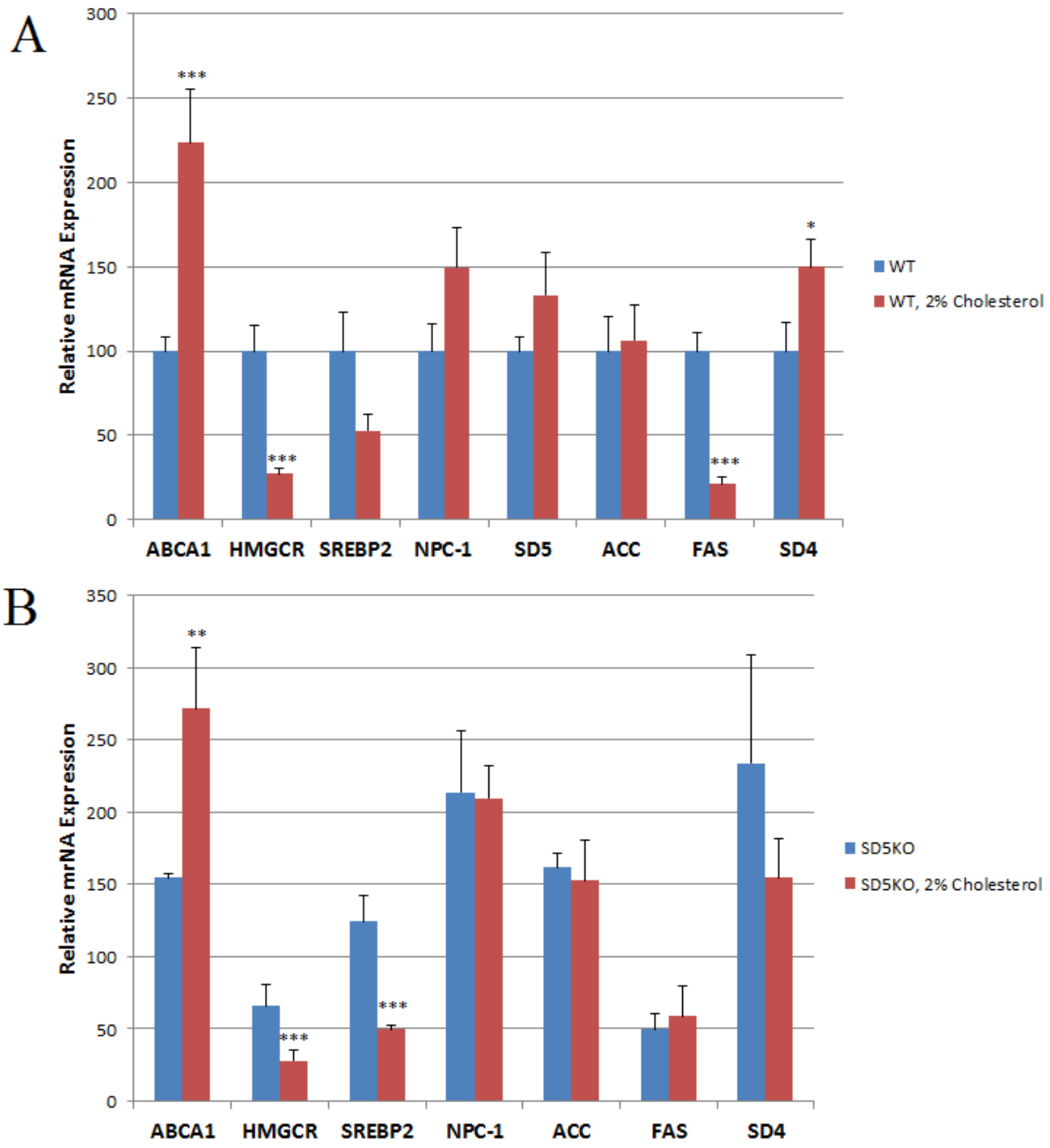

Figure 9. Relative mRNA expression levels in mouse livers in response to being fed a chow diet or a 2% Cholesterol diet for 5 days. *Panel A* – Relative mRNA expression of wild type mice fed a chow diet or a 2% cholesterol diet. *Panel B* – Relative mRNA expression of StarD5$^{-/-}$ mice fed a chow diet or a 2% cholesterol diet. * – P<0.1, ** – P<0.05, *** – P<0.01. n = 3.

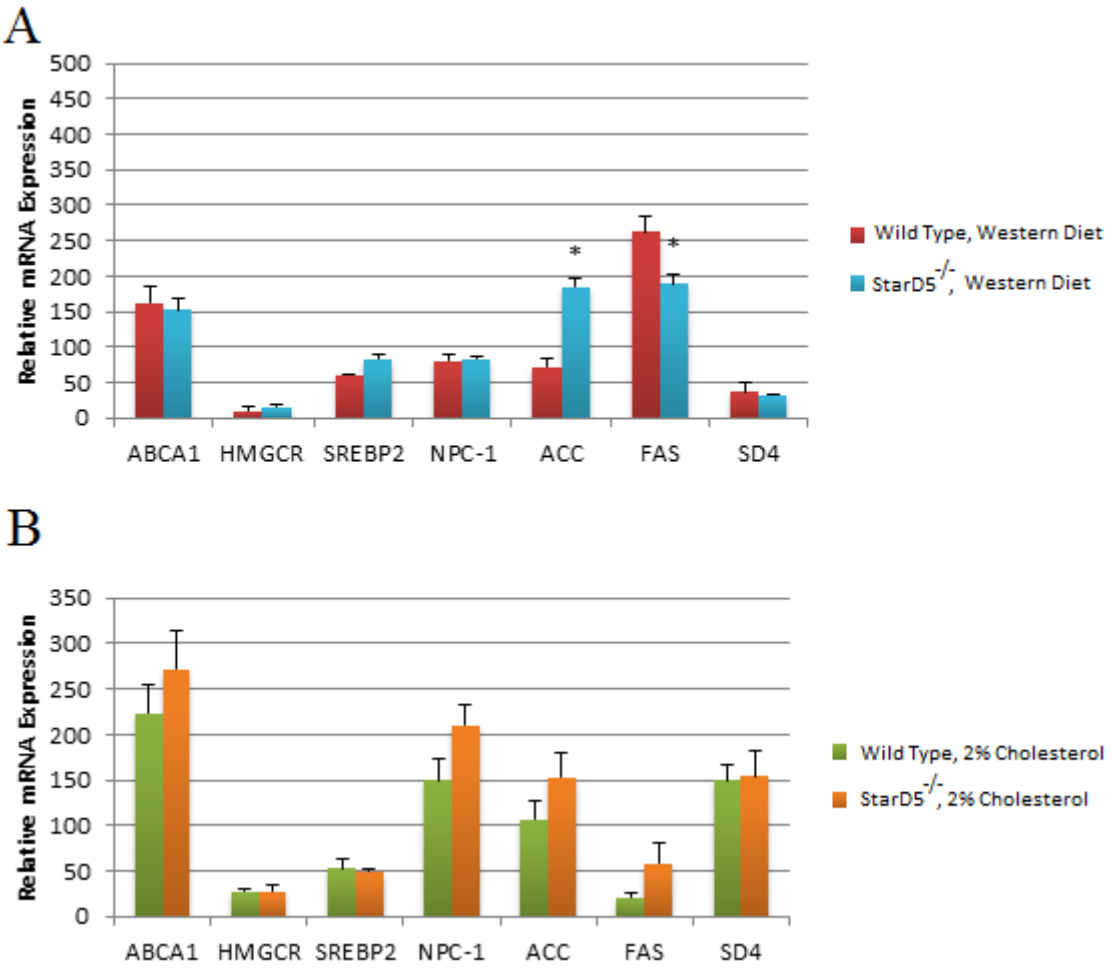

Figure 10. Relative mRNA expression levels for StarD5$^{-/-}$ and wild type mouse livers in response to diet. *Panel A* - The mRNA expression in wild type and StarD5$^{-/-}$ mice in response to being fed a western diet for 8 weeks. *Panel B* - The mRNA expression in wild type and StarD5$^{-/-}$ mice in response to being fed a 2% Cholesterol diet for 5 days. * – P<0.1. n = 3.

2- Overexpression of StarD4 Ameliorates the NPC Phenotype in Mice

StarD4 Overexpression Improves Motor Ability in NPC-1 Mutant Mice as Measured by the Coat Hanger Test

As described in the introduction, knocking out StarD4 in macrophages causes cells to display similar cholesterol levels and distribution as NPC-1 mutant cells **(Figure 1)**. In addition, overexpression of StarD4 appears to normalize the cholesterol distribution in NPC-1 mutant macrophages **(Figure 2)**. For these reasons, StarD4 overexpression was chosen as a potential therapeutic treatment to ameliorate the NPC phenotype. NPC-1 mutant mice were infected with an AAV9-StarD4 virus as described in the Methods section. Ten days following each infection, mice were tested for motor ability with the coat hanger test. Wild type mice had significantly longer hang times than uninfected NPC-1 mutant mice (**Figure 11**). Mice infected with AAV9-StarD4 virus also had longer hang times over uninfected NPC-1 mutant mice. Wild type mice hung for an average of 90 seconds, uninfected NPC-1 mutants mutant hung on for 52 seconds, NPC-1 mutants infected with an AAV9-control virus hung for 56 seconds, NPC-1 mutants infected with AAV9-StarD4 hung for 67 seconds following the first injection and 74 seconds after the second injection.

AAV9-StarD4 Virus Increased Expression of StarD4 in Mouse Livers and Brains

Protein was extracted from the liver samples of uninfected NPC-1 mutants and NPC-1 mutants infected with AAV9-StarD4. These samples run on an acrylamide gel and immunoblotted with a western blotting technique to identify human StarD4 protein. We found that AAV9-StarD4 infected mice expressed 3-fold higher levels of StarD4 protein than in uninfected mutant mice **(Figure 12)**. In addition, we ran qRT-PCR to quantify the expression of

human StarD4 mRNA in the brains of AAV9-StarD4 infected and uninfected NPC-1 mutants. We found that AAV9-StarD4 infected mice had roughly 160% higher mRNA expression of StarD4 than uninfected mice. Despite detecting endogenous StarD4 in both of these tests, these results indicate that infection with AAV9-StarD4 does increase expression of StarD4 in the liver and brain.

Overexpression of StarD4 Does not Impact the mRNA Expression Profile of Key Genes Involved in Cholesterol Metabolism and Transport

RNA was extracted from the livers and brains of wild type mice, NPC-1 mutant mice that were not infected with a virus, NPC-1 mutant mice that were infected with AAV9-control virus, and NPC-1 mutant mice infected with AAV9-StarD4 virus. The relative mRNA expressions of HMG-CoA reductase, ABCA1, and NPC-1, were quantified by qRT-PCR **(Figure 13)**. We found that mice injected with the AAV9-StarD4 virus did not have significantly different mRNA expression from uninjected or AAV9-control virus injected mice for any of the three genes. In the liver, both uninfected and AAV9-StarD4 infected NPC-1 mutants had 170% of the HMG-CoA reductase mRNA expression of wild type mice.

In the brain, HMG-CoA reductase mRNA expression was unchanged between wild types and uninfected NPC-1 mutants; uninfected NPC-1 mutants were at 95% of the HMG-CoA reductase expression of wild types. We also found no difference in ABCA1 mRNA expression between wild types and uninfected NPC-1 mutant. NPC-1 levels show a slight correlation. In AAV9-StarD4 infected NPC-1 mutants, mRNA expression of NPC-1 is 90% of that in wild types. This is compared to uninfected NPC-1 mutants and NPC-1 mutants infected with AAV9-

control virus, which have NPC-1 mRNA expression at about 60% of wild type expression. However, this slight difference is not statistically significant.

Cholesterol and Triglyceride Levels Decrease is Response to StarD4 Overexpression in NPC-1 Mutant Mice

To further explore the impact of StarD4 overexpression on the NPC phenotype, we measured triglyceride, free, and total cholesterol from brain and liver samples of NPC-1 mutant mice. We found that NPC-1 mutant mice infected with AAV9-StarD4 virus had lower levels of total and free cholesterol than uninfected NPC-1 mutant mice. In the liver **(Figure 14)**, AAV9-StarD4 injected NPC-1 mutants have 0.8 ng of total cholesterol per µg of protein while uninjected NPC-1 mutants have 1.7 ng/µg of protein. Free cholesterol levels are very similar- AAV9-StarD4 injected NPC-1 mutants have 0.7 ng of free cholesterol per µg of protein, while uninjected NPC-1 mutants have 1.6 ng/µg of protein.

Brain cholesterol levels also show this pattern **(Figure 15)**. AAV9-StarD4 injected NPC-1 mutants have 4.7 ng of total cholesterol per µg of protein while uninjected NPC-1 mutants have 13.1 ng/µg of protein. Again, free cholesterol levels are very similar to total cholesterol levels- AAV9-StarD4 injected NPC-1 mutants have 5.1 ng of free cholesterol per µg of protein, while uninjected NPC-1 mutants have 13.1 ng/µg of protein.

Triglyceride levels followed a similar pattern in the liver but not in the brain. In the liver NPC-1 mutants injected with AAV9-StarD4 virus had 1.8 ng of cholesterol per µg of protein, while uninfected NPC-1 mutants had 5.3 ng of triglycerides per µg of protein.

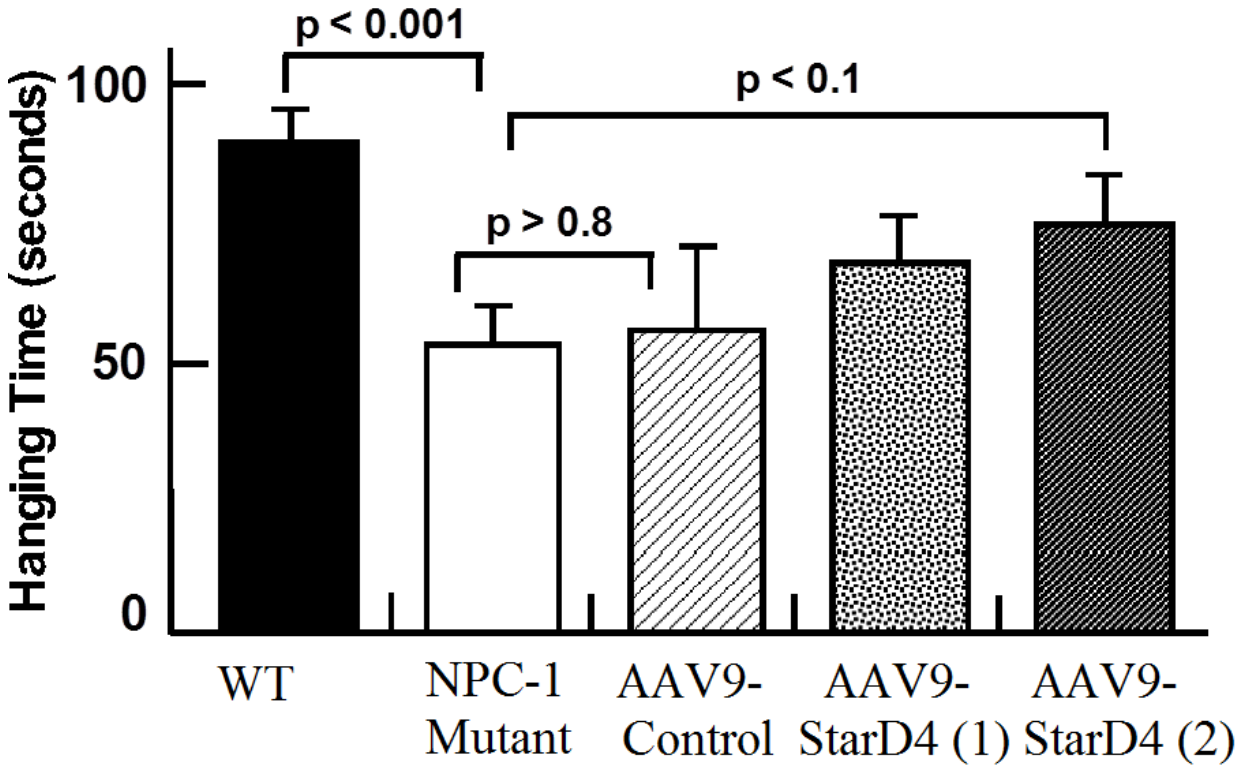

Figure 11. StarD4 overexpression improves motor ability in NPC-1 mutant mice. Wild Type, NPC-1 mutant mice, NPC-1 mutant mice injected with AAV9-control virus, and NPC-1 mutant mice injected with AAV9-StarD4 virus as described in methods were subjected to the coat hanger test to test their motor abilities. Wild type – n=7, NPC-1 mutants – n=7, AAV9-Control – n=3, AAV9-StarD4 (1) – n=7 AAV9-StarD4 (2) – n=6.

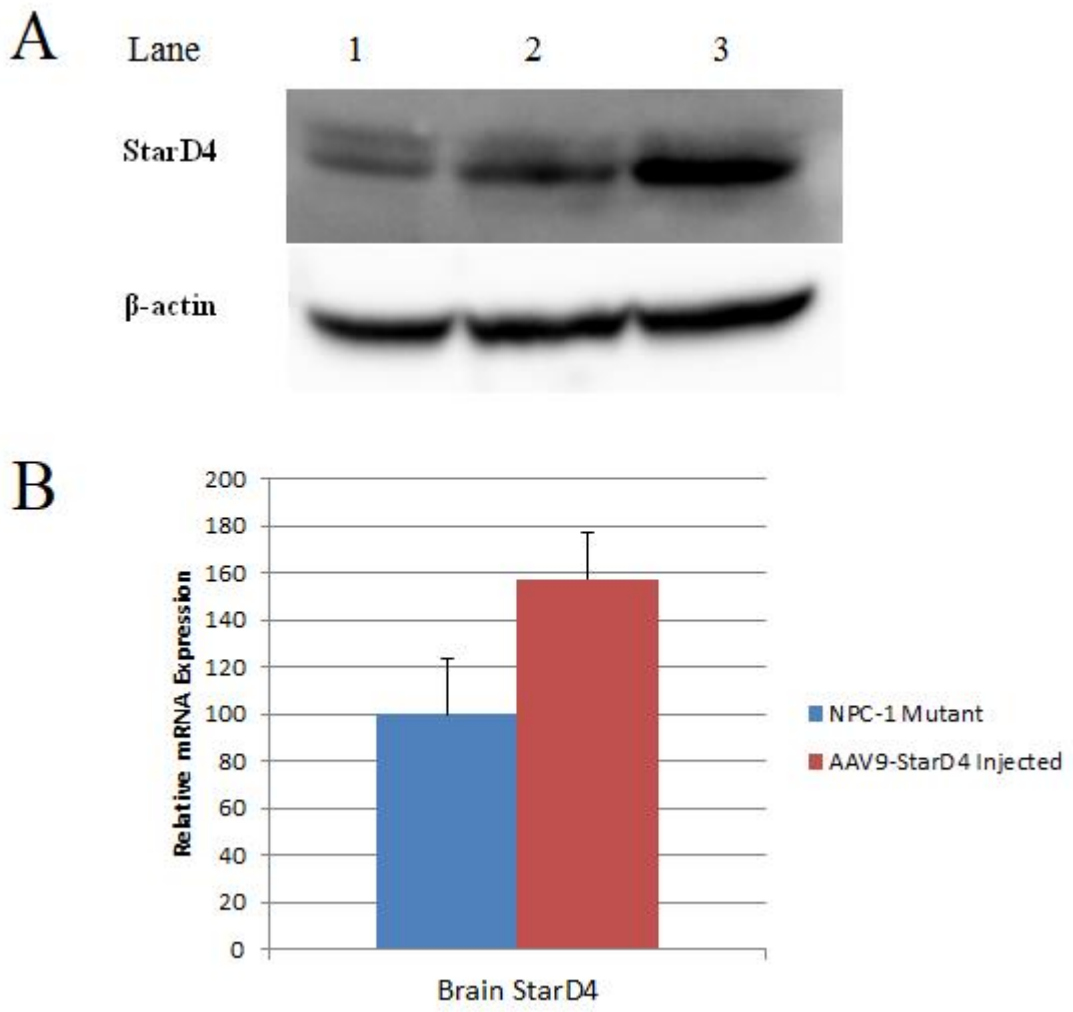

Figure 12. AAV9-StarD4 infection increases StarD4 expression in NPC-1 mutant mouse livers and brains. *Panel A, Lane 1* – Liver from an NPC-1 mutant mouse infected with AAV9-control virus. *Lane 2* - Liver from an NPC-1 mutant mouse harvested after the first AAV9-StarD4 virus injection. *Lane 3* - Liver from an NPC-1 mutant mouse harvested after the second AAV9-StarD4 virus injection. *Panel B* – Relative mRNA expression of StarD4 in the brain between uninjected NPC-1 mutants and AAV9-StarD4 Injected NPC-1 mutants. NPC-1 mutant – n = 4, AAV9-StarD4 Injected – n = 7.

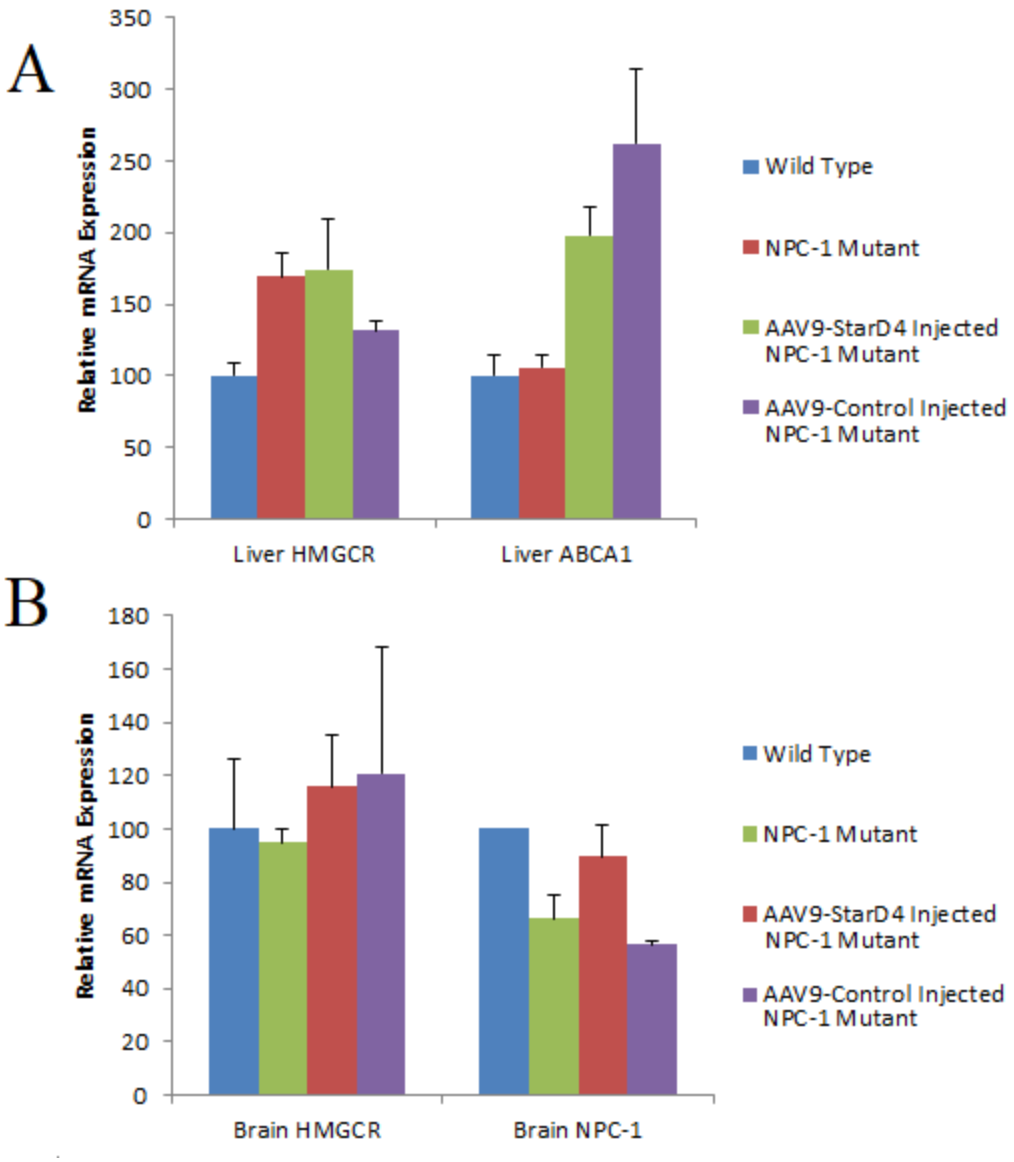

Figure 13. Relative mRNA expression of genes in wild type, uninfected NPC-1 mutant mice, AAV9-control virus infected NPC-1 mutant mice, and AAV9-StarD4 virus infected NPC-1 mutant mice. *Panel A* – Relative mRNA expression of genes in the liver. *Panel B* – Relative mRNA expression of genes in the brain. Wild type - n=4, NPC-1 Mutant - n=4, StarD4 Injected - n=7, Control Injected - n=3.

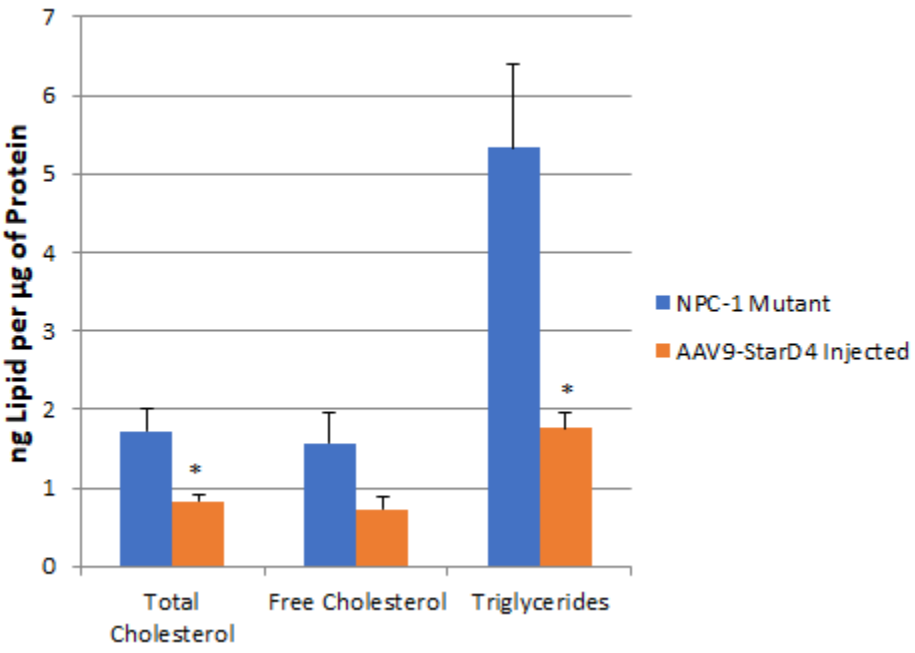

Figure 14. Total cholesterol, free cholesterol, and triglyceride concentrations of uninfected and StarD4 infected NPC-1 mutant mice in the liver. * – P<0.1. Uninjected mutants - n=4, AAV9-StarD4 injected - n=7.

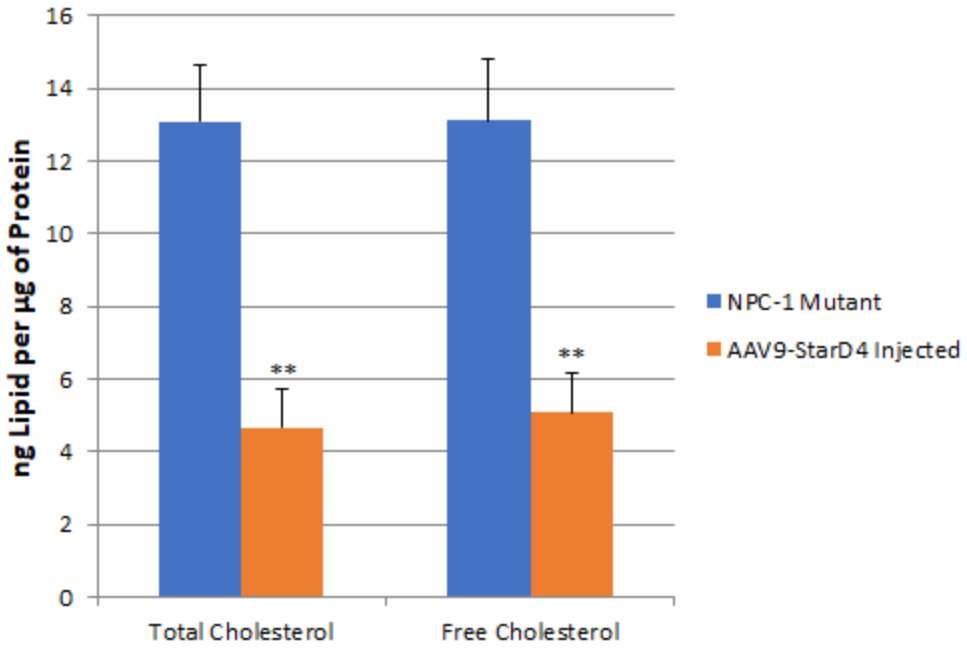

Figure 15. Total and free cholesterol concentrations of uninfected and StarD4 infected NPC-1 mutant mice in the brain. * – P<0.1, ** – P<0.05. Uninjected mutants - n=4. StarD4 injected - n=7.

3- StarD5 Overexpression Ameliorates the NPC Phenotype

ALOD4 Purification and Labelling*

As described in the Methods section, Ni-NTA column fractions were run on an acrylamide gel and stained with coomassie blue dye in order to identify which fractions contained ALOD4* protein (**Figure 16)**. We found that most of the ALOD4* was being eluted between the second and sixth elution. We also stained the original lysate and flowthrough, confirming that most of the ALOD4* had been captured by the column. Following the labelling process, fALOD4* was run on an acrylamide gel for coomassie staining and fluorescent imaging. The protein was detected by both methods **(Figure 17)**, confirming that the protein was fluorescently labelled.

NPC-1 Mutant CHO Cells Have Reduced Levels of Accessible Plasma Membrane Cholesterol Compared to CHO Wild Types

The results presented in this and the following section were selected from a set of representative experiments. We first used fALOD4* to determine the differences in accessible plasma membrane cholesterol levels between wild type CHO and NPC-1 10-3 mutant CHO cells. $1.6x10^6$ wild type and $8x10^5$ NPC-1 mutant cells were grown on 100 mm plates and harvested by incubating in 0.25% trypsin for 10 minutes. Cells were incubated in a series of fALOD4* concentrations and processed by flow cytometry (**Figure 18)**. We found that wild type CHO cells had roughly 2-fold higher levels of accessible plasma membrane cholesterol than NPC-1 mutant CHO cells.

StarD5 Overexpression Increases Accessible Plasma Membrane Cholesterol Levels in Wild Type and NPC-1 Mutant CHO Cells

Next, we looked at the impacts of infecting CHO cells with STAR domain proteins on accessible plasma membrane cholesterol. CHO Wild type and NPC-1 10-3 mutant cells were either left uninfected or infected with 3000 viral particles of StarD5 and StarD4 adenovirus and harvested by incubating in accutase cocktail for 5 minutes. This was done to control the impact of proteolytic cleavage on staining by fALOD4*. More aggressive cleavage techniques could expose cholesterol domains that would ordinarily not be reached by fALOD4*, or could remove the most exposed domains entirely. Accutase is a less aggressive proteolytic cocktail that offered a greater degree of consistency in this experiment. Lysates of CHO cells were run on an acrylamide gel and immunoblotted with a western blotting technique, in order to detect overexpression of StarD4 and StarD5 **(Figure 19)**. We found that cells infected with a StarD4 adenovirus had higher levels of StarD4 protein, while cells infected with a StarD5 adenovirus had higher levels of StarD5 protein.

We once again found that wild type CHO cells had 2-fold higher levels of accessible plasma membrane cholesterol than NPC-1 mutant CHO cells. StarD4 infected wild types and StarD4 infected mutants had very similar accessible plasma membrane cholesterol levels compared to uninfected cells (not shown). However, StarD5 overexpression dramatically increased accessible plasma membrane cholesterol levels. StarD5 overexpression caused a greater increase in accessible plasma membrane cholesterol in wild type cells, where StarD5 overexpression caused an 11-fold increase in accessible plasma membrane cholesterol levels, compared to mutants, where StarD5 overexpression caused a roughly 4-fold increase in accessible plasma membrane cholesterol levels (**Figure 20)**.

The Overexpression of StarD5 Lowers the mRNA Expression of HMG-CoA Reductase in NPC-1 Mutant Mice

The success of increasing accessible plasma membrane cholesterol levels by overexpressing StarD5 in CHOs led us to attempt a preliminary experiment in which StarD5 was overexpressed in NPC-1 mutant mice using a StarD5 adenovirus. Two mice were injected five times over the course of three days with a total of $4.23x10^{10}$ StarD5 adenovirus. One mouse was harvested three days after the first injection. The second mouse was harvested seven days after the first injection. RNA was extracted from the livers of the two infected NPC-1 mutant mice as well as livers of same-age uninfected NPC-1 mutant mice. We used qRT-PCR to determine the relative mRNA expression of three genes **(Figure 21)**. HMG-CoA reductase mRNA expression was markedly lower in the StarD5 injected NPC-1 mutant mice than in uninfected NPC-1 mutant mice. The NPC-1 mutant mouse harvested 3 days after the initial injection had 38% the HMG-CoA reductase expression of uninfected NPC-1 mutant mice, while the NPC-1 mutant mouse harvested 7 days after infection had an even lower level of expression, at 22%. We did not see any differences in the mRNA expression of uninfected NPC-1 mutants and StarD5 infected mutants for ABCA-1 and NPC1. The StarD5 infected NPC-1 mutants harvested 7 days after infection had 78.7% of the expression of NPC-1 mRNA and 117% of the expression of ABCA-1 mRNA compared in uninfected NPC-1 mutant mice.

The Overexpression of StarD5 Lowers Cholesterol and Triglyceride Levels in NPC-1 Mutant Mice

We measured the total cholesterol and triglyceride concentrations in the livers of uninfected and StarD5 infected NPC-1 mutant mice. We found that the mouse harvested 7 days

after infection with StarD5 adenovirus had much lower levels of cholesterol and triglycerides compared to uninfected NPC-1 mutants. Uninfected NPC-1 mutant livers had 1.1 ng of cholesterol per μg of protein, while StarD5 infected NPC-1 mutants had 0.5 ng/μg of protein. Similarly, uninfected NPC-1 mutant livers had 4.6 ng of triglycerides per μg of protein, while StarD5 infected NPC-1 mutants had 1.8 ng/ μg of protein.

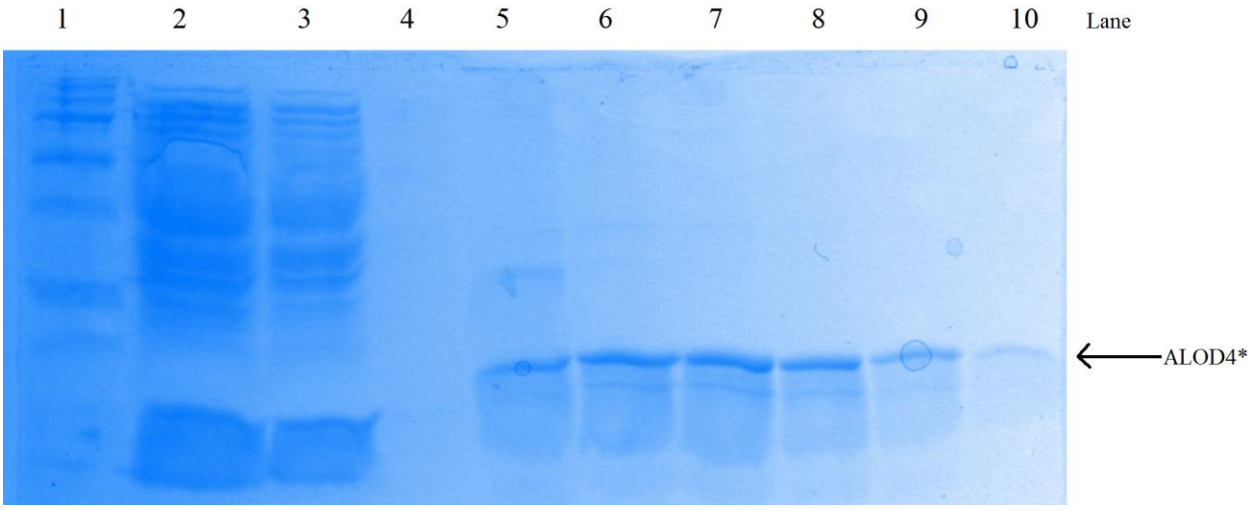

Figure 16. Coomassie staining of the ALOD4* purification process. *Lane 1* - Ladder. *Lane 2* – Cell lysate before running through Ni-NTA column. *Lane 3* - Flowthrough of the Ni-NTA column. *Lanes 4-10:* 2 mL fractions of ALOD4* eluted in 400 mM imidazole.

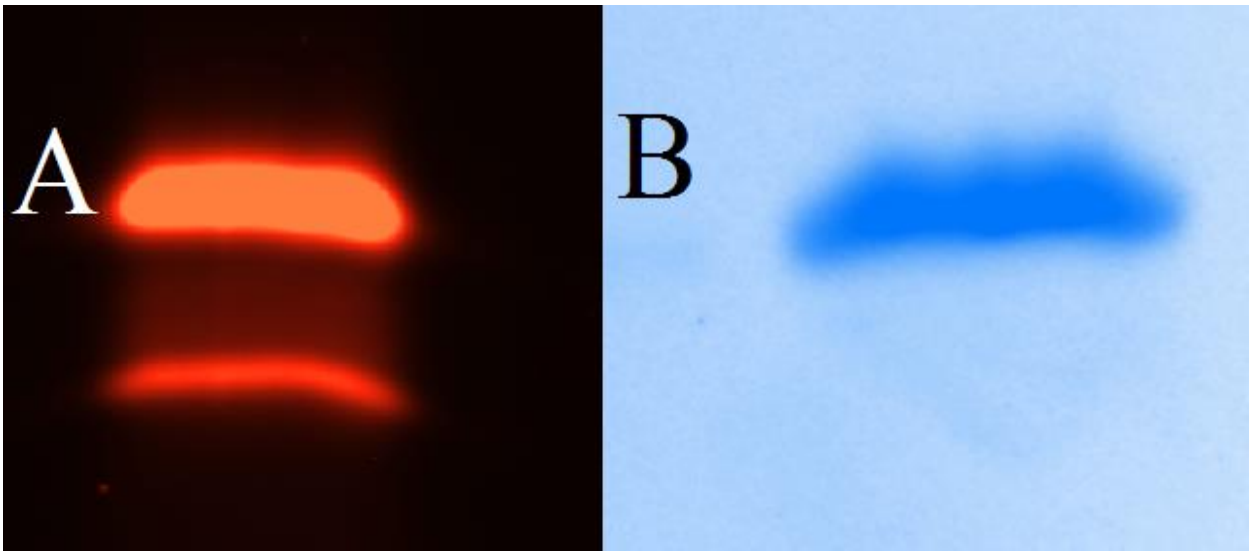

Figure 17. Fluorescent imaging and coomassie staining of fALOD4*. *Panel A* - 100 ng of fALOD4* was ran on a 12% acrylamide gel and imaged for fluorescence. *Panel B* - Coomassie staining of fALOD4*.

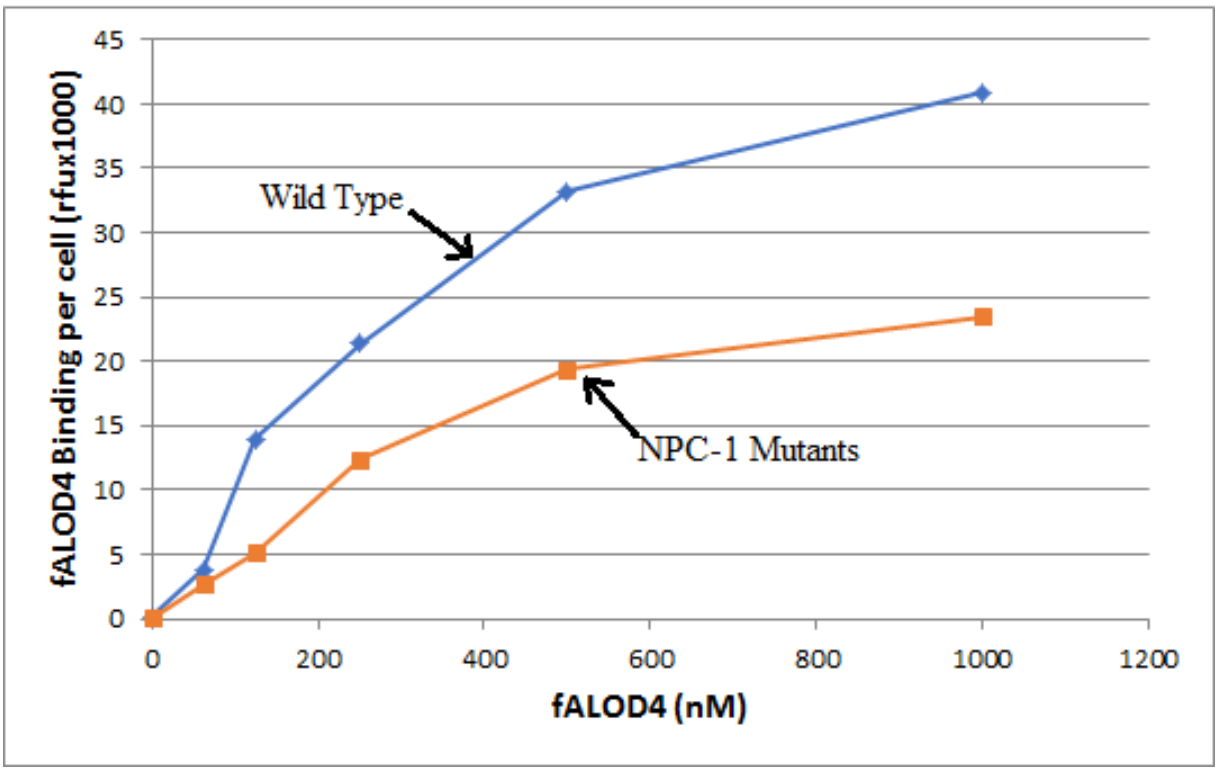

Figure 18. Quantification of accessible plasma membrane cholesterol in CHO wild type and NPC-1 10-3 mutant cells. A concentration curve of fALOD4* was used to quantify accessible plasma membrane cholesterol in CHO wild type and NPC-1 mutant cells.

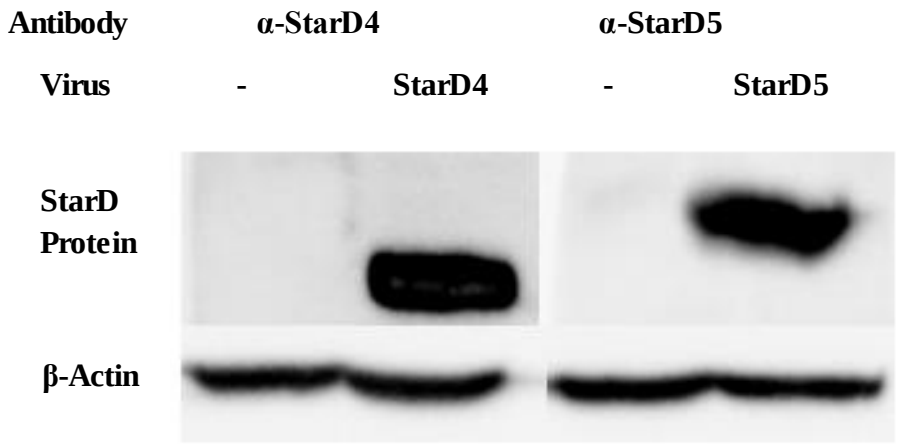

Figure 19. Western blots of protein extracts from CHO cells used to detect overexpression of StarD proteins by infection with adenovirus. CHO wild type cells were infected with StarD4 and StarD5 adenovirus. Lysates from these cells were stained with antibody specific to StarD4, StarD5, and β-Actin.

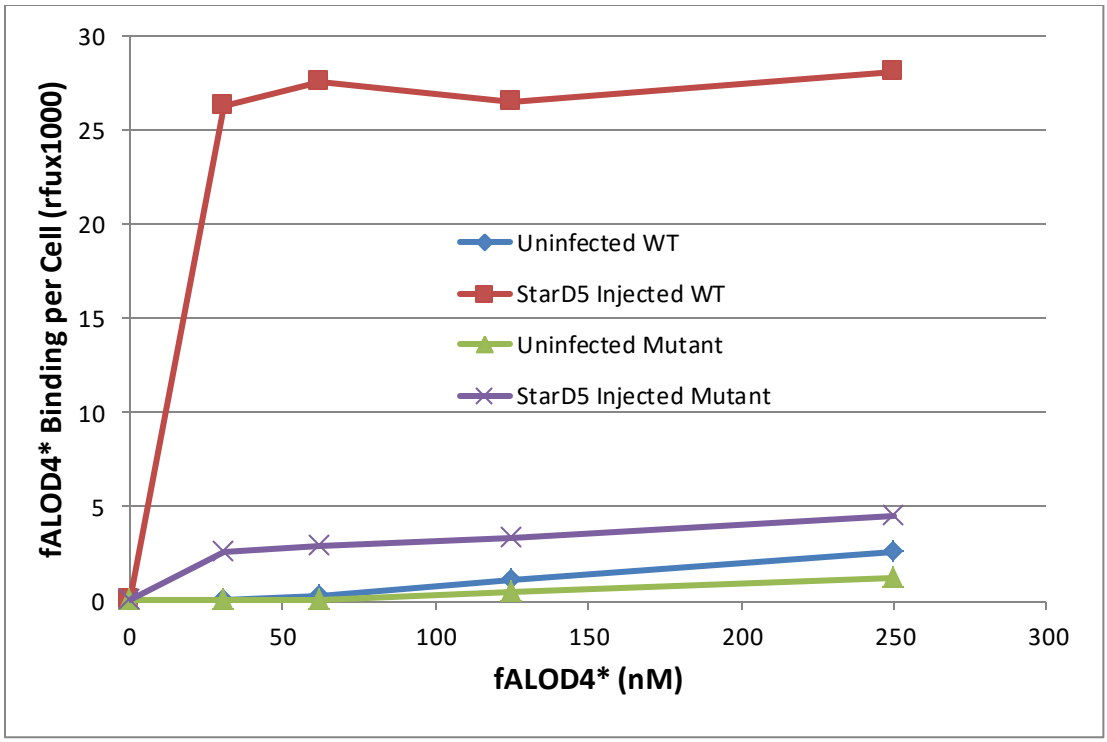

Figure 20. Quantification of accessible plasma membrane cholesterol in CHO wild type and NPC-1 10-3 mutant cells infected with StarD5 adenovirus. A concentration curve of fALOD4* was used to quantify accessible plasma membrane cholesterol in wild type and NPC-1 mutant CHO cells that were uninfected or infected with StarD5 adenovirus.

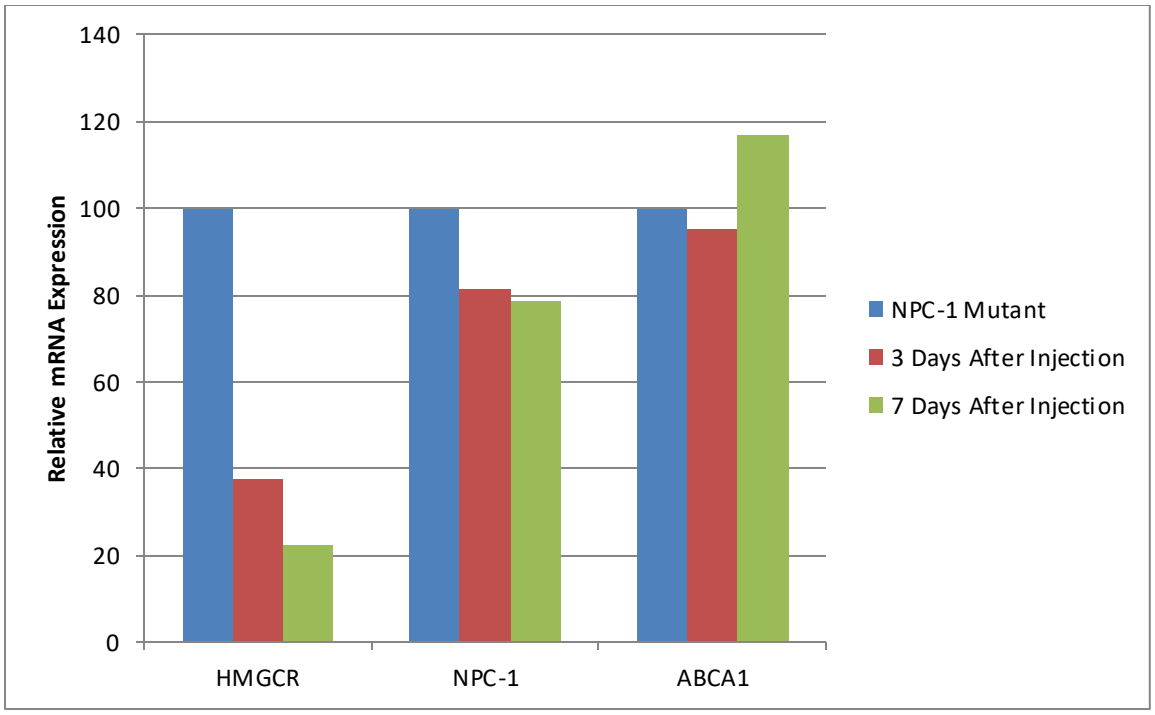

Figure 21. Relative mRNA expression in the livers uninjected and StarD5 injected NPC-1 mutant mice. qRT-PCR was used to determine the relative mRNA expression of HMG-CoA reductase, NPC-1, and ABCA1 in uninjected and StarD5 injected NPC-1 mutant mice. Uninjected - n=2, 3 Days After Injection - n=1, 7 Days After Injection - n =1.

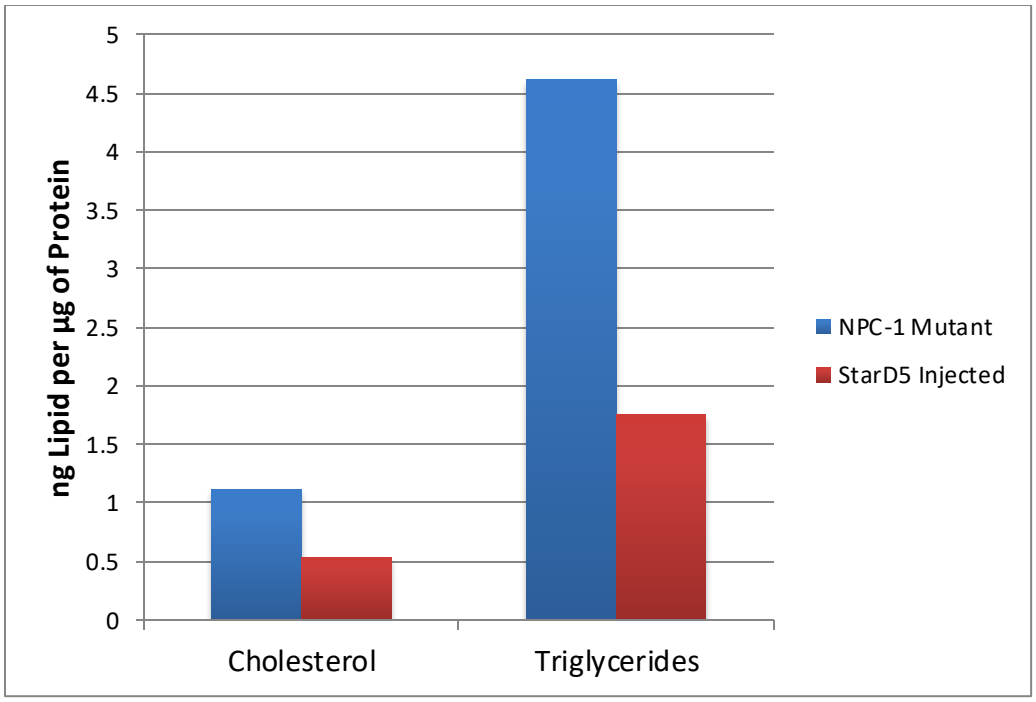

Figure 22. Total cholesterol and triglyceride concentrations of uninfected and StarD5 infected NPC-1 mutant mice in the liver. Uninfected NPC-1 mutants - n=2, StarD5 infected NPC-1 mutants - n=1.

4- Characterization of StarD5 Chaperone Proteins

Immunoprecipitation of StarD5 and Associated proteins from HeLa Cells Infected with a StarD5 Adenovirus

While we have found that overexpressing StarD5 can have impacts on plasma membrane and possibly ER cholesterol levels, there are gaps in our understanding of StarD5 mediated cholesterol transport. StarD5 does not have any known chaperone proteins, and identifying these chaperones would shed light on how StarD5 moves around the cell and transports cholesterol. To investigate this, we infected HeLa cells with a StarD5 adenovirus and incubated in either FBS or LPDS media. We also infected HeLa cells with a control adenovirus and incubated those in FBS media. For each treatment we treated a set of HeLa cells with formaldehyde to crosslink StarD5 to nearby proteins. We used immunoprecipitation to capture StarD5 and any associated proteins, ran the purified protein extracts on an acrylamide gel and stained them with coomassie dye **(Figures 23, 24)**.

In addition to the main StarD5 band, many much fainter bands were detected above StarD5 in both gels. The bottom band is the Flag peptide used to elute the protein. Mass Spectrometry analysis of these fainter bands in the gel in **Figure 24** identified a large number of proteins in these faint upper bands (**Figure 25**). A few of the most promising candidates for a StarD5 chaperone protein were selected for consideration in future studies **(Table 2)**.

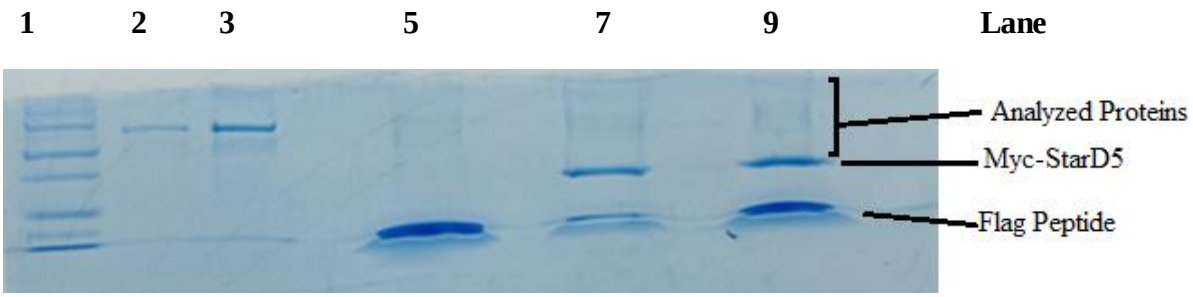

Figure 23. Lysates of StarD5 infected HeLa cells were purified by IP to isolate StarD5 and its potentially associated proteins. *Lane 1* – Ladder. *Lane 2* - 50 ng BSA standard. *Lane 3* - 100 ng BSA standard. *Lane 5* – HeLa cells infected with a control adenovirus and incubated in FBS media. *Lane 7* - HeLa cells infected with a StarD5 adenovirus and incubated in FBS media. *Lane 9* – Hela cells infected with a StarD5 adenovirus and incubated in LPDS media.

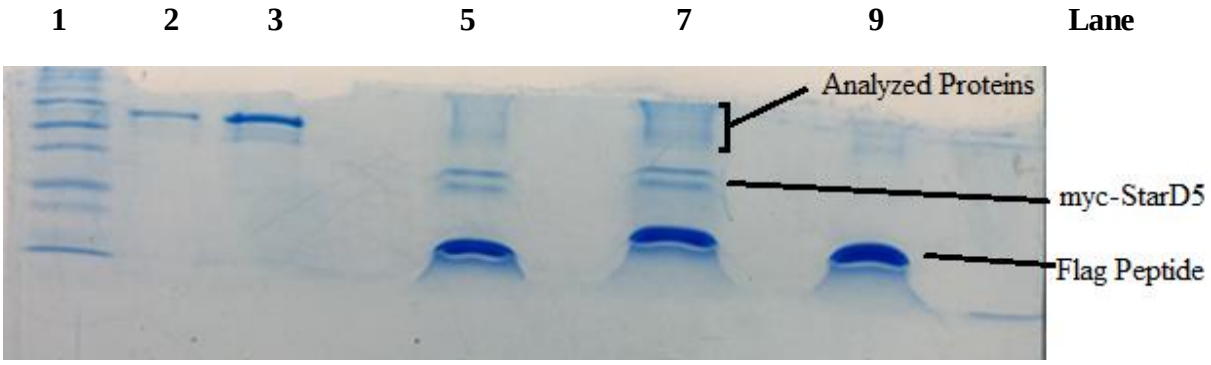

Figure 24. Lysates of StarD5 infected, formaldehyde crosslinked HeLa cells were purified by IP to isolate StarD5 and its potentially associated proteins. *Lane 1* - Ladder. *Lane 2* - 50 ng BSA standard. *Lane 3* - 100 ng BSA standard. *Lane 5* – HeLa cells infected with a control adenovirus and incubated in FBS media. *Lane 7* - HeLa cells infected with a StarD5 adenovirus and incubated in FBS media. *Lane 9* – Hela cells infected with a StarD5 adenovirus and incubated in LPDS media.

gi	Ref ID	Protein defLine	Protein pValue	FBS	LPDS	
17318569	NP_006112.2	keratin 1 [Homo sapiens]	51.179	12 (35)	21 (66)	2
40354192	NP_000412.2	keratin 10 [Homo sapiens]	34.483	7 (12)	10 (23)	2
47132620	NP_000414.2	keratin 2a [Homo sapiens]	31.519	5 (12)	10 (15)	2
55956899	NP_000217.2	keratin 9 [Homo sapiens]	29.658	11 (42)	11 (38)	2
89064520	XP_947550.1	PREDICTED: similar to Pyruvate kinase, isozymes M	13.208	1 (1)	5 (8)	2
20143914	NP_003310.2	titin isoform N2-B [Homo sapiens]	13.160	7 (7)	4 (4)	2
20149594	NP_031381.2	heat shock 90kDa protein 1, beta [Homo sapiens]	10.827	2 (4)	4 (5)	2
27465517	NP_775109.1	keratin 6 isoform K6e [Homo sapiens]	10.482	2 (5)	4 (8)	2
17986283	NP_006000.2	tubulin, alpha 3 [Homo sapiens]	9.813	2 (6)	4 (8)	2
4503571	NP_001419.1	enolase 1 [Homo sapiens]	9.390	3 (3)	X	1
63029937	NP_001017963.1	heat shock protein 90kDa alpha (cytosolic), cl	8.306	1 (2)	2 (2)	2
5729877	NP_006588.1	heat shock 70kDa protein 8 isoform 1 [Homo sapiens	7.663	2 (2)	2 (2)	2
27436940	NP_774959.1	reelin isoform b [Homo sapiens]	7.339	4 (4)	2 (2)	2
56090139	NP_001007566.1	TRK-fused [Homo sapiens]	7.235	3 (5)	1 (1)	2
4507729	NP_001060.1	tubulin, beta 2 [Homo sapiens]	7.031	3 (5)	2 (4)	2
4503483	NP_001952.1	eukaryotic translation elongation factor 2 [Homo s	6.690	1 (1)	3 (3)	2
19923466	NP_057417.2	splicing coactivator subunit SRm300 [Homo sapiens	6.410	2 (2)	3 (3)	2
5174735	NP_006079.1	tubulin, beta, 2 [Homo sapiens]	6.326	1 (1)	3 (4)	2
93102379	NP_061027.2	low density lipoprotein-related protein 1B [Homo	5.995	4 (4)	1 (1)	2
42415529	NP_963868.1	solute carrier family 4, anion exchanger, member	5.785	2 (2)	3 (3)	2
10947122	NP_064693.1	ATP-binding cassette, sub-family C, member 9 isof	5.783	2 (2)	2 (2)	2
32967601	NP_066267.2	ankyrin 3 isoform 1 [Homo sapiens]	5.763	2 (2)	3 (3)	2
45597458	NP_778253.1	keratin 1B [Homo sapiens]	5.598	2 (5)	1 (1)	2
13876382	NP_001363.1	dynein, axonemal, heavy polypeptide 9 isoform 2 [	5.548	5 (5)	X	1
74048554	NP_653091.2	cancer susceptibility candidate 5 isoform 2 [Homo	5.462	X	3 (3)	1
55741750	NP_065075.1	solute carrier family 39 (zinc transporter), memb	5.315	1 (1)	3 (3)	2
6005938	NP_009055.1	utrophin [Homo sapiens]	5.299	1 (1)	3 (3)	2
32307124	NP_006525.2	nuclear receptor coactivator 3 isoform b [Homo sa	5.288	4 (4)	X	1
92110053	NP_443128.2	CUB and Sushi multiple domains 2 [Homo sapiens]	5.277	3 (3)	2 (2)	2
65288071	NP_073585.8	tensin-like SH2 domain containing 1 [Homo sapiens	5.227	4 (4)	X	1
29294651	NP_803187.1	dicer1 [Homo sapiens]	5.204	2 (2)	2 (2)	2
57634534	NP_055950.1	nucleoporin 205kDa [Homo sapiens]	5.158	2 (2)	2 (2)	2
75677365	NP_065928.2	dynein heavy chain domain 3 [Homo sapiens]	5.134	1 (1)	4 (4)	2
16306568	NP_075045.2	poly(A) polymerase gamma [Homo sapiens]	5.117	1 (1)	3 (3)	2
55741857	NP_056327.3	dynein, axonemal, heavy polypeptide 1 [Homo sapie	5.056	2 (2)	2 (2)	2
38455427	NP_006421.2	chaperonin containing TCP1, subunit 4 (delta) [Hom	5.042	X	2 (2)	1
38505213	NP_073739.2	YTH domain containing 2 [Homo sapiens]	4.954	3 (3)	1 (1)	2
50345997	NP_001420.2	E1A binding protein p300 [Homo sapiens]	4.942	4 (4)	X	1
41281518	NP_055661.2	hypothetical protein LOC9897 [Homo sapiens]	4.872	2 (2)	2 (2)	2
45237197	NP_073746.1	pleckstrin homology domain containing, family G (	4.755	1 (1)	2 (2)	2
63175654	NP_659496.2	fucokinase [Homo sapiens]	4.718	3 (3)	1 (1)	2
29029632	NP_004295.2	anaplastic lymphoma kinase Ki-1 [Homo sapiens]	4.693	1 (1)	3 (3)	2
74319833	NP_004645.2	ubiquitin specific protease 9, Y-linked [Homo sap	4.678	3 (3)	1 (1)	2
27545313	NP_115946.2	ubiquitin specific protease 38 [Homo sapiens]	4.675	2 (2)	1 (1)	2
83367077	NP_078966.2	mucin 16 [Homo sapiens]	4.626	3 (3)	1 (1)	2
71902540	NP_000042.3	ataxia telangiectasia mutated protein isoform 1 [	4.615	1 (1)	2 (2)	2

Figure 25. Samples from the coomassie stained gel were analyzed by MS for StarD5 associated proteins. Protein p-Value is the confidence that the protein is present. pValues below 5 indicate low confidence in the presence of protein. The numbers in the 5th and 6th columns indicate the number of unique peptides detected and (in parenthesis) the total number of times these peptides were scanned for cells incubated in FBS and LPDS respectively.

Table 2. Candidates for StarD5 Chaperone Proteins, chosen from proteins in Figure 25. Protein p-Value is the confidence that the protein is present. pValues below 5 indicate low confidence in the presence of protein. The numbers in the 4th and 5th columns indicate the number of unique peptides detected and (in parenthesis) the total number of times these peptides were scanned for cells incubated in FBS and LPDS respectively.

Protein	ID	p-Value	FBS	LPDS
TRK-fused	NP_001007566.1	7.235	3 (5)	1 (1)
Low density lipoprotein related protein 1B	NP_061027.2	5.995	4 (4)	1 (1)
ATP-binding cassette, sub-family C, member 9 isoform	NP_064693.1	5.783	2 (2)	2 (2)
Ankyrin 3 isoform 1	NP_066267.2	5.763	2 (2)	3 (3)

Discussion

Gene expression analysis of the StarD5$^{-/-}$ mice shows that they have a lower HMG-CoA reductase mRNA expression, and a higher NPC-1 and ABCA1 mRNA expression. These responses correlate with our understanding of StarD5. Without StarD5, cholesterol accumulates inside the cells and possibly in the ER. A high level of ER cholesterol would prevent the activation of SREBP-2, which would trigger downregulation of HMG-CoA reductase. mRNA expression of ABCA1 and NPC-1 is likely increased due to upregulation by LXR, which is activated by oxysterols produced in response to high levels of free cholesterol.

Interestingly, when mice were fed a 2% cholesterol diet we do not see the same pattern of mRNA expression. For example, in StarD5$^{-/-}$ mice FAS mRNA expression is unchanged in response to a 2% cholesterol diet. Under a 2% cholesterol diet, wild type and StarD5$^{-/-}$ mice had a similar level of mRNA for every gene we tested. This is likely because when mice are fed a 2% cholesterol diet, there are high levels of intracellular cholesterol in both wild type and StarD5$^{-/-}$ mice. High levels of cholesterol trigger same regulatory pathways in both mouse strains, leading to the same regulatory patterns.

In macrophages StarD5$^{-/-}$ and wild type mice have similar levels of mRNA in all of the genes we tested. StarD5 is highly expressed in macrophages, so knocking out StarD5 was expected to affect mRNA expression in these cells. This lack of response in macrophages suggests that despite its high expression in this cell type, StarD5 is not as important in macrophages as had been previously thought.

NPC-1 mutant mice infected with AAV9-StarD4 virus had improved motor ability over uninfected and AAV9-control virus infected mutants, as demonstrated by the coat hanger test. These results are supported by the cholesterol and triglyceride levels. AAV9-StarD4 injected NPC-1 mutant mice had lower levels of total and free cholesterol than uninjected NPC-1 mutant mice in both the liver and the brain. There is a decrease in the level triglycerides in the liver, but not in the brain. However, in the brain the NPC phenotype is most apparent in the cerebellum [36]. We did not isolate regions of the brain, so we do not have a complete picture of how StarD4 overexpression affects the NPC phenotype in the brain.

The results from the behavioral test and cholesterol assays suggest that overexpression of StarD4 affects the NPC phenotype. It was anticipated that changes in motor ability and lipid levels would be accompanied by a change in mRNA expression. However, our qRT-PCR experiments gave some unexpected results. Mice infected with AAV9-StarD4 did not have a significantly altered mRNA expression for any of the genes tested, aside from StarD4 itself. This raises the question of where exactly StarD4 is transporting cholesterol to within the cell, since the transport of cholesterol in the ER would normally result in the downregulation of HMG-CoA reductase. StarD4 may be transporting cholesterol to a specific ER domain where it does not affect HMG-CoA reductase expression. Another possibility is that StarD4 is transporting cholesterol to the endocytic recycling compartment. It is important to note that this experiment only involved seven AAV9-StarD4 infected mice, so these anomalous results could disappear with a higher sample size.

The NPC phenotype is detectable in CHO cells through accessible plasma membrane cholesterol levels. Quantification of accessible plasma membrane cholesterol with fALOD4* revealed that wild type CHOs have more accessible plasma membrane cholesterol than NPC-1

mutants. This was expected- NPC disease causes on accumulation of cholesterol in the late endosomes while cholesterol levels in the ER and plasma membrane decrease. We also found that overexpression of StarD5 with a StarD5 adenovirus in CHO cells dramatically increases accessible plasma membrane cholesterol levels. This is the most convincing evidence yet that StarD5 transports cholesterol to the plasma membrane. StarD5 triggers a much larger increase in accessible plasma membrane cholesterol in CHO wild types than in NPC-1 mutants, which suggests that cholesterol is not being transported from the late endosomes. NPC-1 mutants have high levels of cholesterol in the late endosomes, so if StarD5 transported cholesterol from the late endosomes one would expect that the overexpression of StarD5 would trigger a larger increase in accessible plasma membrane cholesterol in NPC-1 mutants.

In NPC-1 mutant mice, we found that the overexpression of StarD5 with a StarD5 adenovirus reduced HMH-CoA reductase mRNA expression in the liver. This is accompanied by a decrease of cholesterol and triglycerides in the liver in response to StarD5 overexpression. It should be noted that this is a very preliminary experiment, involving only two infected mice. Regardless, these results are very promising and indicate that overexpression of StarD5 has the potential to treat NPC. A decline in HMG-CoA reductase expression suggests that cholesterol levels in the ER increased in response to StarD5 overexpression. This is contrary to what would be expected if cholesterol was being transported from the ER to the plasma membrane. The results of our CHO experiments, while using a different cell type, suggest that StarD5 is not taking cholesterol from the late endosomes either. The endocytic recycling compartment is a likely candidate for a source of cholesterol for StarD5 mediated cholesterol transport, as it is rich in cholesterol and StarD4 has been shown to transport cholesterol from it to the plasma membrane. We also found that despite its impact on the NPC phenotype in NPC-1 mutant mice,

overexpression of StarD4 in CHO cells does not affect accessible plasma membrane cholesterol levels. There are still a number of possibilities for where StarD4 could be transporting cholesterol, such as inaccessible domains of the plasma membrane, the endocytic recycling compartment, and certain domains of the ER **(Figure 26)**.

We were able to isolate proteins that were potentially associated with StarD5 and narrowed these detected proteins down to a short list of candidates for a StarD5 chaperone. Since LPDS triggers the movement of StarD5 to the plasma memrane, an ideal candidate protein would be more strongly associated with StarD5 after exposure to LPDS. In addition, any known chaperone protein that was associated with StarD5 would be a candidate. Unfortunately, I did not have the time or resources to persue this project further.

StarD5 activation has the potential to act as a therapy for NPC. However, it is clear that more research is needed in this area. This includes a more robust experiment involing the injection a larger number of NPC-1 mutant mice with an AAV9-StarD5 virus. Alternative behavioral tests could give more accurate information on the neurodegeneration of NPC-1 mutant mice [49]. Harvesting the cerebellum separately could help show a more complete picture of how StarD4 and StarD5 overexpression affects the NPC phenotype in the brain Further research is also needed to understand the function of StarD4 and StarD5. While I have provided a list of potential StarD5 chaperones, my work here is only the first step in identifying a StarD5 chaperone protein. The identification of a StarD5 chaperone would be a major step in understanding the intracellular transport of cholesterol, and would also be useful in further research on the use of StarD5 overexpression to treat NPC.

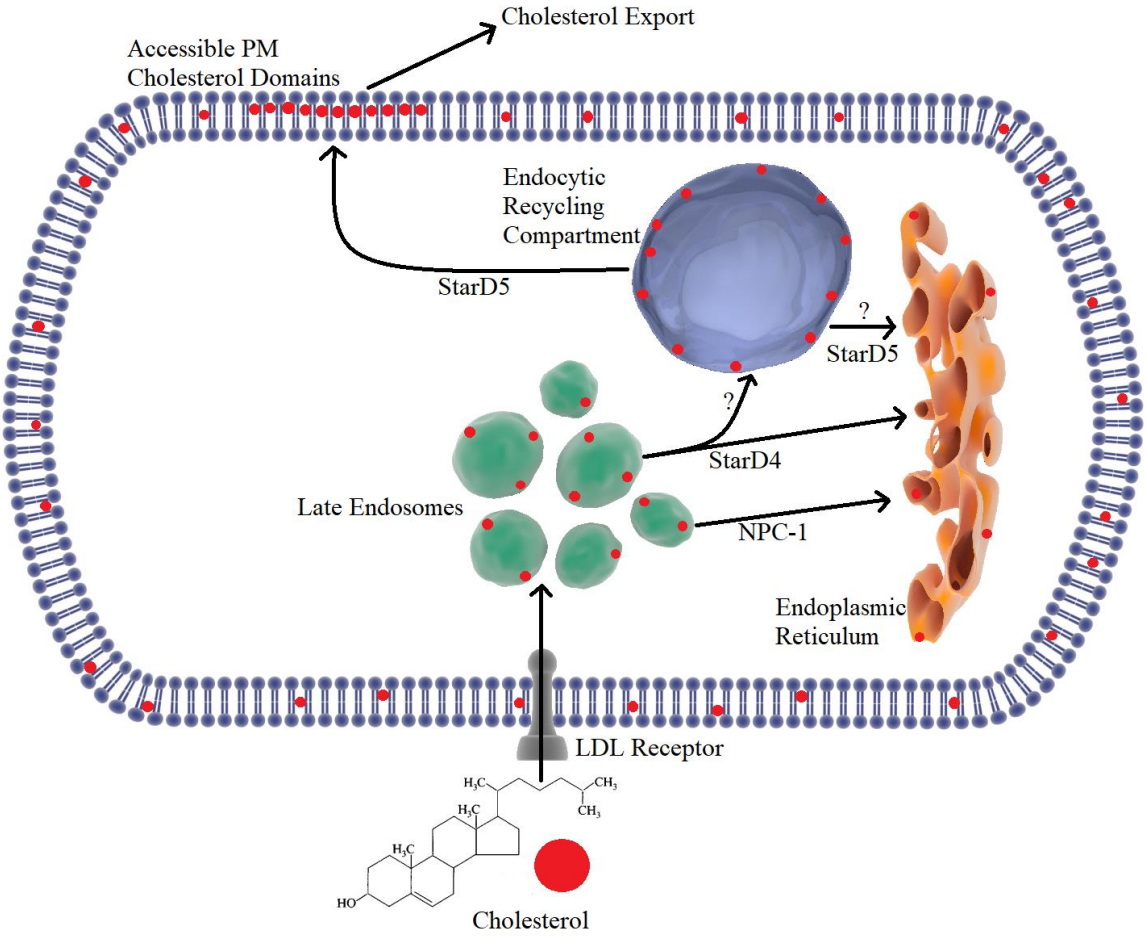

Figure 26. A diagram describing StarD4 and StarD5 mediated cholesterol transport, and a suggested mechanism for amelioration of the NPC phenotype.

Conclusions

Our results shed some light on the function of StarD5. In StarD5$^{-/-}$ mouse livers, several genes have a significantly altered level of mRNA expression, likely due to the buildup of cholesterol within the cell. We have found the strongest evidence yet that StarD5 transports cholesterol to the plasma membrane, possibly from the endocytic recycling compartment. We have collected a list of potential StarD5 chaperone proteins, but more research will be needed in order to identify StarD5 chaperones.

StarD4 and StarD5 have both shown promise in ameliorating the impacts of NPC disease. We found that overexpression of StarD4 in NPC-1 mutant mice improved motor ability and lowered levels of intracellular cholesterol in the liver and brain. Overexpression of StarD5 in CHO wild type and mutant cells triggered the movement of cholesterol to accessible domains of the plasma membrane. In a preliminary experiment, we found that overexpression of StarD5 lowered mRNA expression of HMG-CoA reductase in the liver, as well as lowering levels of cholesterol and triglycerides in the liver. However, due to the low sample size of this experiment, a broader mouse study will be needed.

List of References

List of References

1. Fleisher, S. and B. Fliesher, *Membrane Diversity in the Rat Hepatocyte*. 1977, MTP Press.
2. Buhaescu, I. and H. Izzedine, *Mevalonate pathway: a review of clinical and therapeutical implications.* Clin Biochem, 2007. **40**(9-10): p. 575-84.
3. Dashti, M., et al., *A phospholipidomic analysis of all defined human plasma lipoproteins.* Sci Rep, 2011. **1**: p. 139.
4. Vaz, F.M. and S. Ferdinandusse, *Bile acid analysis in human disorders of bile acid biosynthesis.* Mol Aspects Med, 2017.
5. Wong, J., C.M. Quinn, and A.J. Brown, *SREBP-2 positively regulates transcription of the cholesterol efflux gene, ABCA1, by generating oxysterol ligands for LXR.* Biochem J, 2006. **400**(3): p. 485-91.
6. Horton, J.D., J.L. Goldstein, and M.S. Brown, *SREBPs: activators of the complete program of cholesterol and fatty acid synthesis in the liver.* J Clin Invest, 2002. **109**(9): p. 1125-31.
7. Hannah, V.C., et al., *Unsaturated fatty acids down-regulate srebp isoforms 1a and 1c by two mechanisms in HEK-293 cells.* J Biol Chem, 2001. **276**(6): p. 4365-72.
8. Gosmain, Y., et al., *Regulation of SREBP-1 expression and transcriptional action on HKII and FAS genes during fasting and refeeding in rat tissues.* J Lipid Res, 2005. **46**(4): p. 697-705.
9. Tall, A.R., P. Costet, and N. Wang, *Regulation and mechanisms of macrophage cholesterol efflux.* J Clin Invest, 2002. **110**(7): p. 899-904.
10. Rasmussen-Torvik, L.J., et al., *Ideal cardiovascular health is inversely associated with incident cancer: the Atherosclerosis Risk In Communities study.* Circulation, 2013. **127**(12): p. 1270-5.
11. Barquera, S., et al., *Global Overview of the Epidemiology of Atherosclerotic Cardiovascular Disease.* Arch Med Res, 2015. **46**(5): p. 328-38.

12. *Correction.* Circulation, 2015. **131**(24): p. e535.

13. Banach, M., et al., *Impact of statin therapy on coronary plaque composition: a systematic review and meta-analysis of virtual histology intravascular ultrasound studies.* BMC Med, 2015. **13**: p. 229.

14. Ramkumar, S., A. Raghunath, and S. Raghunath, *Statin Therapy: Review of Safety and Potential Side Effects.* Acta Cardiol Sin, 2016. **32**(6): p. 631-639.

15. Collins, R., et al., *Interpretation of the evidence for the efficacy and safety of statin therapy.* Lancet, 2016. **388**(10059): p. 2532-2561.

16. Fitzgerald, K., D. Kallend, and A. Simon, *A Highly Durable RNAi Therapeutic Inhibitor of PCSK9.* N Engl J Med, 2017. **376**(18): p. e38.

17. van der Vorst, E.P.C., et al., *HDL and macrophages: explaining the clinical failures and advancing HDL-based therapeutics in cardiovascular diseases?* Expert Rev Cardiovasc Ther, 2017. **15**(5): p. 343-344.

18. Schmitz, G. and T. Langmann, *Structure, function and regulation of the ABC1 gene product.* Curr Opin Lipidol, 2001. **12**(2): p. 129-40.

19. Sene, A., et al., *Impaired cholesterol efflux in senescent macrophages promotes age-related macular degeneration.* Cell Metab, 2013. **17**(4): p. 549-61.

20. Yamauchi, Y., S. Yokoyama, and T.Y. Chang, *Methods for Monitoring ABCA1-Dependent Sterol Release.* Methods Mol Biol, 2017. **1583**: p. 257-273.

21. Bielska, A.A., et al., *Oxysterols as non-genomic regulators of cholesterol homeostasis.* Trends Endocrinol Metab, 2012. **23**(3): p. 99-106.

22. Zhu, X., et al., *Macrophage ABCA1 reduces MyD88-dependent Toll-like receptor trafficking to lipid rafts by reduction of lipid raft cholesterol.* J Lipid Res, 2010. **51**(11): p. 3196-206.

23. Mendez, A.J., et al., *Membrane lipid domains distinct from cholesterol/sphingomyelin-rich rafts are involved in the ABCA1-mediated lipid secretory pathway.* J Biol Chem, 2001. **276**(5): p. 3158-66.

24. Iaea, D.B., et al., *Role of STARD4 in sterol transport between the endocytic recycling compartment and the plasma membrane.* Mol Biol Cell, 2017. **28**(8): p. 1111-1122.

25. Yu, X.H., et al., *NPC1, intracellular cholesterol trafficking and atherosclerosis.* Clin Chim Acta, 2014. **429**: p. 69-75.

26. Rigamonti, E., et al., *Liver X receptor activation controls intracellular cholesterol trafficking and esterification in human macrophages.* Circ Res, 2005. **97**(7): p. 682-9.

27. Marí, M., et al., *Mitochondrial cholesterol accumulation in alcoholic liver disease: Role of ASMase and endoplasmic reticulum stress.* Redox Biol, 2014. **3**: p. 100-8.

28. Soccio, R.E., et al., *The cholesterol-regulated StarD4 gene encodes a StAR-related lipid transfer protein with two closely related homologues, StarD5 and StarD6.* Proc Natl Acad Sci U S A, 2002. **99**(10): p. 6943-8.

29. Calderon-Dominguez, M., et al., *The StarD4 subfamily of steroidogenic acute regulatory-related lipid transfer (START) domain proteins: new players in cholesterol metabolism.* Int J Biochem Cell Biol, 2014. **49**: p. 64-8.

30. Garbarino, J., et al., *STARD4 knockdown in HepG2 cells disrupts cholesterol trafficking associated with the plasma membrane, ER, and ERC.* J Lipid Res, 2012. **53**(12): p. 2716-25.

31. Rodriguez-Agudo, D., et al., *Subcellular localization and regulation of StarD4 protein in macrophages and fibroblasts.* Biochim Biophys Acta, 2011. **1811**(10): p. 597-606.

32. Rodriguez-Agudo, D., et al., *ER stress increases StarD5 expression by stabilizing its mRNA and leads to relocalization of its protein from the nucleus to the membranes.* J Lipid Res, 2012. **53**(12): p. 2708-15.

33. Chang, T.Y., et al., *Niemann-Pick type C disease and intracellular cholesterol trafficking.* J Biol Chem, 2005. **280**(22): p. 20917-20.

34. Cupidi, C., et al., *Role of Niemann-Pick Type C Disease Mutations in Dementia.* J Alzheimers Dis, 2017. **55**(3): p. 1249-1259.

35. Koens, L.H., et al., *Ataxia, dystonia and myoclonus in adult patients with Niemann-Pick type C.* Orphanet J Rare Dis, 2016. **11**(1): p. 121.

36. Kim, M.J., et al., *Substance P immunoreactive cell reductions in cerebral cortex of Niemann-Pick disease type C mouse.* Brain Res, 2005. **1043**(1-2): p. 218-24.

37. Vanier, M.T. and P. Latour, *Laboratory diagnosis of Niemann-Pick disease type C: the filipin staining test.* Methods Cell Biol, 2015. **126**: p. 357-75.

38. Patterson, M.C., et al., *Miglustat for treatment of Niemann-Pick C disease: a randomised controlled study.* Lancet Neurol, 2007. **6**(9): p. 765-72.

39. Tamura, A., K. Nishida, and N. Yui, *Lysosomal pH-inducible supramolecular dissociation of polyrotaxanes possessing acid-labile N-triphenylmethyl end groups and their therapeutic potential for Niemann-Pick type C disease.* Sci Technol Adv Mater, 2016. **17**(1): p. 361-374.

40. Zervas, M., et al., *Critical role for glycosphingolipids in Niemann-Pick disease type C.* Curr Biol, 2001. **11**(16): p. 1283-7.

41. Pipalia, N.H., et al., *Histone deacetylase inhibitor treatment dramatically reduces cholesterol accumulation in Niemann-Pick type C1 mutant human fibroblasts.* Proc Natl Acad Sci U S A, 2011. **108**(14): p. 5620-5.

42. Alam, M.S., M. Getz, and K. Haldar, *Chronic administration of an HDAC inhibitor treats both neurological and systemic Niemann-Pick type C disease in a mouse model.* Sci Transl Med, 2016. **8**(326): p. 326ra23.

43. Underwood, K.W., et al., *Evidence for a cholesterol transport pathway from lysosomes to endoplasmic reticulum that is independent of the plasma membrane.* J Biol Chem, 1998. **273**(7): p. 4266-74.

44. Zincarelli, C., et al., *Analysis of AAV serotypes 1-9 mediated gene expression and tropism in mice after systemic injection.* Mol Ther, 2008. **16**(6): p. 1073-80.

45. Rodriguez-Agudo, D., et al., *Intracellular cholesterol transporter StarD4 binds free cholesterol and increases cholesteryl ester formation.* J Lipid Res, 2008. **49**(7): p. 1409-19.

46. Chakrabarti, R.S., et al., *Variability of cholesterol accessibility in human red blood cells measured using a bacterial cholesterol-binding toxin.* Elife, 2017. **6**.

47. Gay, A., D. Rye, and A. Radhakrishnan, *Switch-like responses of two cholesterol sensors do not require protein oligomerization in membranes.* Biophys J, 2015. **108**(6): p. 1459-69.

48. Das, A., et al., *Three pools of plasma membrane cholesterol and their relation to cholesterol homeostasis.* Elife, 2014. **3**.

49. Maue, R., et al., *A novel mouse model of Neimann-Pick Type C disease carrying a D1005G-Npc1 mutation comparable to commonly observed human mutations*. 2012, Human Molecular Genetics. p. 730-750.

Vita

Tavis Sparrer was born on May 28th, 1992. He grew up in Gloucester, Virginia and earned a B.S. in Biochemistry at Virginia Tech. He worked as a lab technician for two years at the Virginia Institute of Marine Science before entering the Master's program at VCU.